UC Berkeley
UC Berkeley Electronic Theses and Dissertations

Title
State-dependent cortical processing: Cholinergic modulation of visual responses

Permalink
https://escholarship.org/uc/item/8j96f8hg

Author
Goard, Michael

Publication Date
2009

Peer reviewed|Thesis/dissertation

eScholarship.org Powered by the California Digital Library
University of California

State-dependent cortical processing:
Cholinergic modulation of visual responses

by

Michael Phillip Goard

A dissertation submitted in partial satisfaction of the

Requirements for the degree of

Doctor of Philosophy

in

Neuroscience

in the

Graduate Division

of the

University of California, Berkeley

Committee in charge:

Professor Yang Dan, Chair
Professor Frédéric Theunissen
Professor Michael Silver
Professor Michael Gastpar

Fall 2009

State-dependent cortical processing:
Cholinergic modulation of visual responses

Copyright 2009

by

Michael Phillip Goard

Abstract

State-dependent cortical processing:
Cholinergic modulation of visual responses

by

Michael Phillip Goard

Doctor of Philosophy in Neuroscience

University of California, Berkeley

Professor Yang Dan, Chair

The nucleus basalis of the basal forebrain is an essential component of the neuromodulatory system controlling the behavioral state of an animal, and it is thought to play key roles in regulating arousal and attention. However, the effect of NB activation on sensory processing remains poorly understood. Using polytrode recording in rat visual cortex, we show that NB stimulation causes prominent decorrelation between neurons and marked improvement in the reliability of neuronal responses to natural scenes. The decorrelation depends on local activation of cortical muscarinic acetylcholine receptors, while the increased reliability involves distributed neural circuits, as evidenced by NB-induced changes in thalamic responses. Further analysis showed that the decorrelation and increased reliability improve cortical representation of natural stimuli in a complementary manner. Thus, the basal forebrain neuromodulatory circuit, which is known to be activated during aroused and attentive states, acts through both local and distributed mechanisms to improve sensory coding.

Table of contents

Chapter 1. Introduction: State-dependent cortical processing and the roles of cholinergic neuromodulation

1.1 Introduction to cortical processing in rat V1 1
1.2 State-dependent modulation of stimulus-driven responses in sensory cortex 4
1.3 Influence of basal forebrain cholinergic system on cortical state 6
1.4 Effects of acetylcholine on stimulus-driven responses of V1 7
1.5 Summary and motivation 9

Chapter 2. Cholinergic modulation of V1 cortical state and response properties

2.1 Preface 10
2.2 Methods 10
2.3 Stimulation of basal forebrain cholinergic system 12
2.4 Polytrode recording in visual cortex 14
2.5 Effect of nucleus basalis stimulation on cortical LFP 16
2.6 Effect of nucleus basalis stimulation on V1 spatial receptive fields 18
2.7 Effect of nucleus basalis stimulation on orientation tuning and direction selectivity 20
2.8 Summary 22

Chapter 3. Basal forebrain activation enhances cortical coding of natural scenes

3.1 Preface 23
3.2 Methods 23
3.3 NB stimulation decorrelates cortical responses and improves single neuron reliability 25
3.4 Decorrelation mediated by mAChRs 32
3.5 Improved reliability involves distributed changes along the sensory pathway 33
3.6 Basal forebrain activation enhances cortical coding of natural scenes 36
3.7 Summary 38

Chapter 4. Conclusions and implications

4.1 Summary of novel experimental results 39
4.2 Discussion or results 40
4.3 Future directions 42

References 46

Chapter 1. Introduction: State-dependent cortical processing and the role of cholinergic modulation

1.1 Introduction to cortical processing in rat V1

Area V1 is the first processing level of visual inputs to cortex and has been an area of active scientific interest since it was initially characterized by Hubel and Wiesel (Hubel and Wiesel, 1962). It is a useful system for investigating the role of neuromodulation and cortical state on sensory processing because the response properties of V1 neurons are relatively well understood. What follows is a brief description of V1 neuron response properties.

Orientation tuning

David Hubel, while working at Walter Reed hospital, invented the microelectrode by coating sharpened tungsten wires with lacquer insulation, with the very tip exposed to allow electrical conduction. Microelectrodes, with their small recording area and sharp profile, allowed recording from single neurons adjacent to the electrode tip. After moving to Johns Hopkins University, Hubel, in collaboration with Torsten Wiesel, began a long and fruitful research program to characterize the neurons of the visual cortex, for which they were awarded the Nobel Prize in 1981.

When Hubel and Wiesel recorded action potentials from visual cortical neurons of anesthetized cats, one of their first discoveries was that V1 neurons did not respond well to dots of light. This is in contrast to neurons in earlier regions of the visual pathway. Both retinal and lateral geniculate neurons respond optimally to either bright dots with dark surround or dark dots with a bright surround at a specific location in the visual field (**Fig. 1.1a**, top). Visual cortical neurons still exhibit retinotopic properties; that is, they respond preferentially to visual stimuli in a distinct part of the visual field. However, rather than being driven by light or dark dots like retinal and geniculate neurons, V1 neurons respond preferentially to lines, bars or gratings crossing specific areas of the visual field (Hubel and Wiesel, 1962). Hubel and Wiesel hypothesized that this quality of cortical receptive fields was generated by the arrangement of inputs from the lateral geniculate nucleus (LGN; **Fig. 1.1**).

This model has since been confirmed by simultaneous recordings of LGN and V1 neurons (Reid and Alonso, 1995). Furthermore, depending on the arrangement of LGN inputs, a V1 neuron would not respond equally to any line crossing the appropriate part of the visual field, but would respond preferentially to lines of a specific orientation. Thus, when lines or bars are moved across the receptive field at a range of different orientations, the response can be described as a Gaussian centered on a preferred orientation, a property known as orientation tuning (**Fig. 1.2**, bottom). Neurons located in layer 4 of cortex (and to a lesser extent in layer 6), called simple cells, receive direct thalamocortical input, but cells in other layers generally receive input from cortical neurons of similar orientation, such that the orientation tuning is preserved. These cells are labeled complex cells due to their spatially invariant responses (Hubel

and Wiesel, 1962). Thus, orientation tuning is exhibited by the majority, though not all, of V1 cortical neurons.

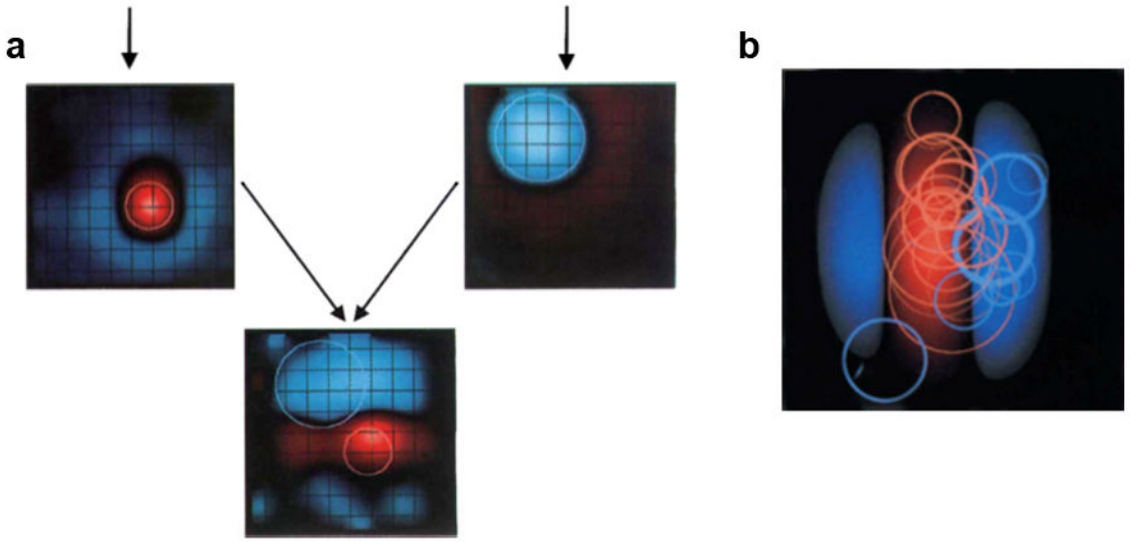

Figure 1.1: Receptive fields of V1 neurons are derived from connections to LGN neurons with aligned receptive fields. (a) Receptive fields of two LGN neurons (top) monosynaptically connected to a V1 neuron (bottom). Red corresponds to excitatory regions of the visual field, blue corresponds to suppressive regions. **(b)** Neurons in V1 are connected only to LGN neurons with appropriately aligned receptive fields. Shown here is a composite receptive field from several V1 neurons that have been rotated and scaled. Red and blue circles show location and polarity of receptive fields from monosynaptically connected LGN cells. Figure adapted from Alonso, Ursey, & Reid (1996) and Reid & Alonso (1995).

Direction Selectivity

Based purely on the orientation tuning of visual neurons, one would expect the responses to a bar moving across the receptive field at the preferred orientation to be the same regardless of the direction of the drift. However, Hubel and Wiesel found that a subset of orientation-tuned neurons also seem to prefer movement in a particular direction, a property with ramifications for downstream processing of visual motion (Hubel and Wiesel, 1962) (**Fig. 1.2b**).

Spatial receptive fields

As noted earlier, visual cortex is arranged into a spatially-specific receptive fields, such that any given region of visual cortex responds to a small area of the visual field. Thus, the receptive field of a neuron can be described as the pattern of light in the visual field that will optimally elicit action potentials from that neuron. Techniques for measuring receptive fields of cortical neurons are an active field of study, but a common approach is to display a noise stimulus to the animal while measuring the responses of a neuron (Marmarelis, 1977; Marmarelis and McCann, 1977). By averaging the stimuli that occurred during action potentials, the researcher can determine the visual stimulus that best excites the neuron of interest. Retina and LGN neurons have been mapped using this method and have been found to have receptive fields in which a light or dark spot is surrounded by an annulus of the opposite polarity, consistent with observed response properties (Barlow, 1953; Hubel and Wiesel, 1961) (**Fig. 1.1**). Determining the receptive fields

of cortical neurons is more difficult, as the regions of visual space activated by bright stimuli and dark stimuli sometimes overlap. However, more advanced methods have revealed that cortical receptive fields are elongated, as would be expected by their orientation preferences (Hubel and Wiesel, 1962; Reid and Alonso, 1995).

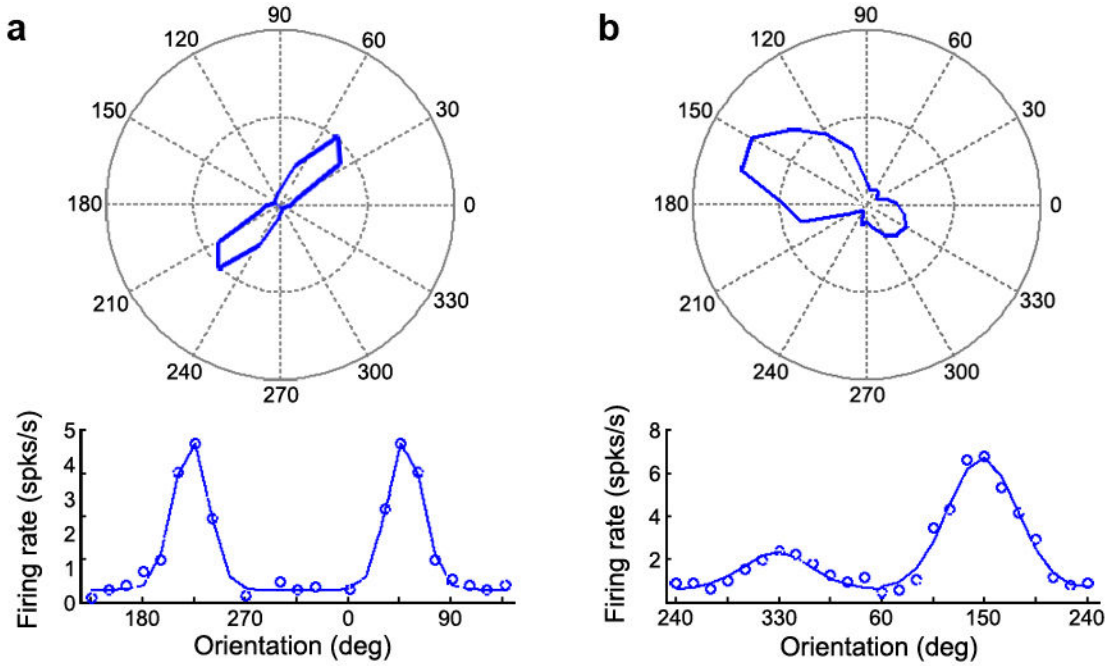

Figure 1.2: Orientation tuning and direction selectivity in V1 neurons. (a) Polar (top) and Cartesian (bottom) plots of the responses of a V1 neuron to oriented gratings in different directions. This neuron is not direction selective. **(b)** Responses of a direction selective neuron.

Responses to natural movies

Parameterized stimuli such as gratings and noise have been useful for determining the response properties of cortical neurons, but natural visual input has a much more complicated statistical structure. In recent years, a concerted effort has been made to understand neural responses to natural stimuli. Several groups have found that cortical neurons exhibit different response properties when exposed to natural scenes than when exposed to noise stimuli (Felsen et al., 2005; Sharpee et al., 2006). Furthermore, cortical responses to natural scenes tend to be unreliable and difficult to predict, perhaps due to the lower contrast and slower temporal frequencies of natural scenes compared to noise stimuli (Kara et al., 2000). Thus, to understand how neuromodulation and cortical state affect visual processing in V1, it is important to consider responses to natural stimuli as well as the more parameterized stimuli traditionally used for receptive field estimation.

The visual system of the rodents

Rodents are nocturnal and rely heavily on olfactory and whisker sensation. Since they are not primarily visual animals, cats and monkeys have traditionally been favored for studies of visual

cortical processing. However, since rodents are more amenable to genetic analysis and acute studies involving electrical stimulation and pharmacological manipulations, recent research has focused on characterizing the visual cortex of mice (Niell and Stryker, 2008) and rats (Girman et al., 1999). The findings suggest that while rodents appear to be missing some higher processing areas, the primary visual cortex functions in an analogous manner to that of cats and primates. The most striking differences between rodents and traditional organisms are that rodents have larger receptive fields, less spatial acuity, and lack orientation columns [which are also missing in some highly visual animals, such as squirrels, tree shrews, and squirrel monkeys (Heimel et al., 2005)]. Rodent V1 neurons do exhibit sharp orientation tuning, direction selectivity, spatial and temporal frequency tuning, and typical contrast response functions (Girman et al., 1999; Niell and Stryker, 2008). Thus, on the whole, rodent V1 neurons are largely similar to cat or primate V1 neurons despite the shifts in response selectivity. Furthermore, rodents are capable of solving visual discrimination tasks in order to obtain a reward (Prusky et al., 2000), demonstrating that they have fully functioning visual systems despite any differences between species. These characteristics make rodents a practical model for studying early visual processing.

1.2 State-dependent modulation of stimulus-driven responses in sensory cortex

Although much is known about how feedforward inputs drive neural responses in area V1, it is not yet possible to accurately predict the spike train of a cell based purely on the stimulus. Recent research has demonstrated that the variability in sensory responses is largely due to spontaneous membrane potential fluctuations generated in the absence of sensory input (Arieli et al., 1996; Petersen et al., 2003). In fact, one study used voltage-sensitive dye imaging to examine the multi-neural responses of a region of V1 to sensory inputs (Arieli et al., 1996). They found that the response could be predicted with much higher accuracy if the spontaneous activity at the time of stimulus presentation was added directly to the average response to that stimulus (**Fig. 1.3**). This suggests that ongoing cortical dynamics may act to strongly shape sensory-driven responses.

Internally generated cortical dynamics are not a novel observation. In fact, well before the first microelectrode recording in cortex, Hans Berger used electroencephalography (EEG) to measure large scale averaged electrical activity from the scalp of human volunteers, and observed distinct waveforms depending on the behavioral state of the subject (Berger, 1929; Penfield and Erickson, 1941). In general, subjects in deep sleep tend to show large, low frequency oscillations in their EEG waveforms while alert subjects exhibit smaller amplitude, higher frequency activity (**Fig. 1.4**). Even in the awake subjects, profound differences in the EEG waveform are observed depending on whether the subject is drowsy, restful, or excited (**Fig. 1.4**). Given the differences in sensory processing ability in each of these states, it does not seem farfetched to imagine that the endogenous modulations might reflect different cortical processing states. This could occur either because the oscillations are directly affecting the fidelity with which the cortex encodes sensory information, or because the oscillations are a hallmark of other changes in the cortical circuit, such as differences in neural excitability or functional connectivity.

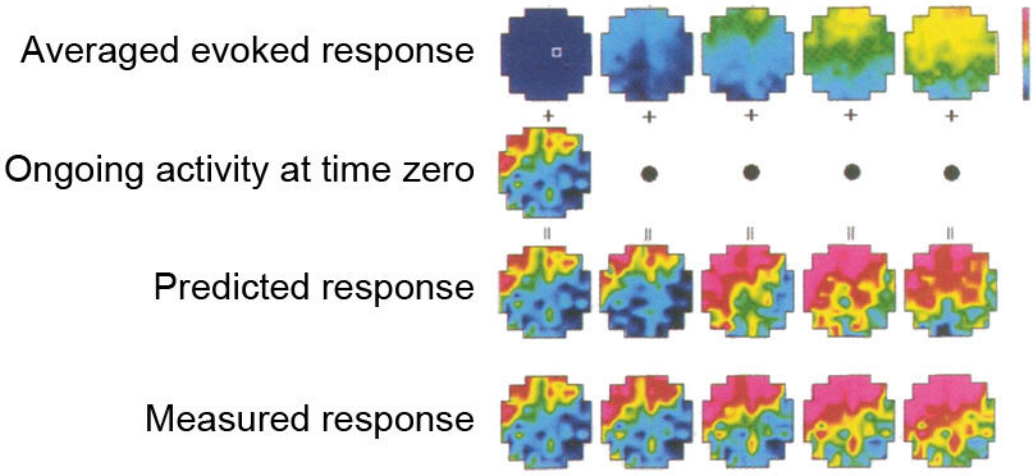

Figure 1.3: Visual cortical responses influenced by spontaneous activity at time of visual stimulation. Measured voltage-sensitive dye responses from a visual stimulus (bottom row) are predicted with higher accuracy if the ongoing activity at the time of stimulation (second row) is added to the averaged evoked response to the stimulus (top row) to generate the predicted response (third row). Adapted from Arieli, Sterkin, Grinvald & Aertsen (1996).

This is supported by evidence that the receptive fields of V1 neurons are larger during synchronized EEG states (high amplitude, low frequency activity) than during desynchronized states (low amplitude, high frequency activity), suggesting that spontaneous cortical dynamics can modulate visual acuity (Worgotter et al., 1998). By patching single neurons, several labs have demonstrated that sensory evoked spiking is modulated by the spontaneous membrane potential fluctuations driven by ongoing cortical activity (Petersen et al., 2003; Sanchez-Vives and McCormick, 2000). Thus, during Up states (a depolarized membrane potential that occurs during slow cortical oscillations), sensory events are less likely to generate spiking than during Down states (a less depolarized membrane potential at a different phase of the oscillation). A further study demonstrated that when a rat shifts in behavioral state from quiet wakefulness to active whisking, the EEG desynchronizes and the membrane potentials of different cells become less synchronized (Poulet and Petersen, 2008). This results in an increased ratio of sensory driven membrane fluctuations to spontaneous fluctuations, which would presumably result in more reliable coding of sensory stimuli. Taken together, these results demonstrate that ongoing network dynamics play a role in shaping cortical responses to sensory stimuli. However, it is not well understood whether cortical dynamics are modulated in a behaviorally relevant manner, and how the changes in cortical dynamics might be internally triggered.

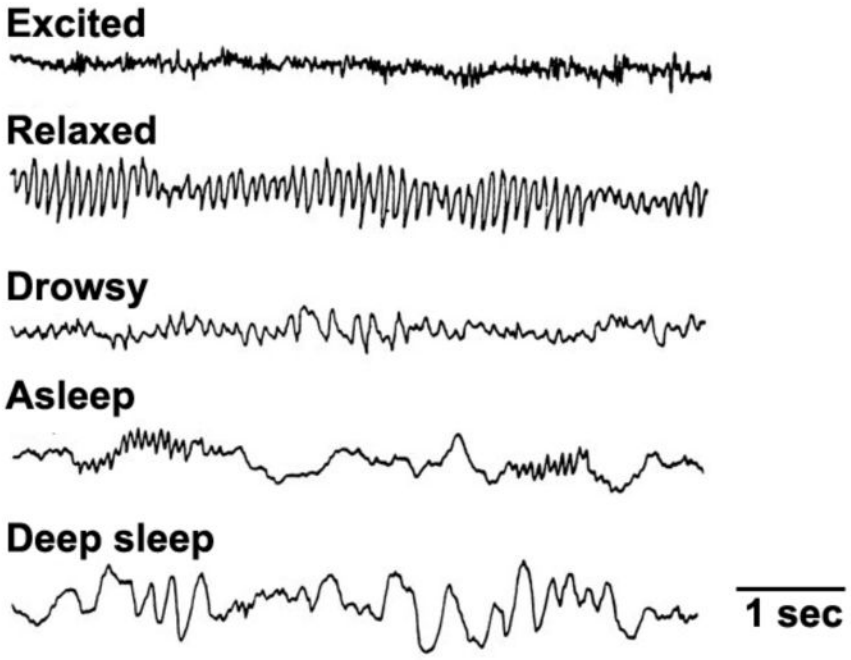

Figure 1.4: Behavioral states are characterized by distinct EEG waveforms. EEG traces contain different frequency composition depending on whether the subject is awake or asleep, as well as when the subject is differentially aroused. Adapted from Penfield & Erickson (1941).

1.3 Influence of basal forebrain cholinergic system on cortical state

A candidate physiological system for modulating cortical dynamics in a behaviorally relevant manner should meet the following criteria: (1) it should be a discrete physiological system that can be selectively activated or suppressed, and should have cortical targets (2) the endogenous activity of the system should mirror the behavioral state of the animal, (3) lesions of the system should disrupt behaviorally-modulated cortical function, and (4) activation/suppression of the system should observably modulate cortical dynamics. The cholinergic system of the basal forebrain projecting to cortex, also known as the nucleus basalis of Meynert, meets all of these criteria.

The cholinergic cells of nucleus basalis form a small cluster in the basal forebrain and constitute the sole subcortical source of acetylcholine to sensory cortex (Lehmann et al., 1980). The nucleus projects widely and promiscuously throughout the cerebral cortex, and can increase cortical acetylcholine levels transiently or over long timescales (Lehmann et al., 1980). Thus, the nucleus basalis is a discrete neuromodulatory system that is anatomically placed in a manner to selectively regulate cortical dynamics.

The cholinergic cells are active during waking and REM sleep, but not during slow wave sleep or in anesthetized states (Jones, 2008; Lee et al., 2005). Furthermore, in the awake animal, the cholinergic cells become more active as a function of arousal and task demand (Buzsaki et al., 1988; Laplante et al., 2005; Parikh et al., 2007). Activation of the nucleus basalis can also facilitate responses to sensory stimuli and has been implicated in enhancing cortical plasticity (Froemke et al., 2007) and inducing activity-dependent remapping (Bakin and Weinberger, 1996; Kilgard and Merzenich, 1998). Thus, the endogenous activity of the nucleus basalis is highly

correlated to the level of behavioral arousal [in fact, some physiological effects of behavioral arousal, such as increased heart rate and respiration, appear to be generated by nucleus basalis activation (McLin et al., 2002)].

Lesion studies of nucleus basalis function have been carried out using excitotoxic chemicals such as ibotenic acid, which kills all nucleus basalis cells, or cholinergic neuron-specific toxin 192 IgG-saporin. These studies revealed deficits in visual perception (Muir et al., 1994), attention (Muir et al., 1994), and memory (Page et al., 1991) in both rats and primates. The memory deficits are more controversial, as they have been reported with non-specific excitotoxic lesions but are less evident with cholinergic-specific 192 IgG-saporin lesions, but the perceptual and attentional deficits are robust (Everitt and Robbins, 1997). Also, perceptual and attentional deficits seen in humans with Alzheimer's disease, which causes damage to cholinergic basal forebrain neurons, closely mimic those seen in animals with selective nucleus basalis lesions (Everitt and Robbins, 1997). These results demonstrate that damage to the basal forebrain cholinergic system disrupts behaviorally-modulated function of the visual system.

Finally, abundant research has demonstrated that nucleus basalis activation or suppression dramatically affects cortical dynamics, specifically by acting on muscarinic acetylcholine receptors (mAChRs). One study found that lesion of nucleus basalis with Ibotenic acid resulted in an increase in cortical slow waves (Buzsaki et al., 1988). This result was mimicked by a mAChR antagonist, scopolamine, applied directly to cortex (Buzsaki et al., 1988). Furthermore, electrical stimulation of the nucleus basalis results in marked changes to the cortical EEG. Specifically, nucleus basalis stimulation reduces high amplitude, low frequency activity and increases small amplitude, high frequency activity (Buzsaki et al., 1988; Metherate et al., 1992), similar to the effect of arousal. By patching single cortical neurons, researchers found that nucleus basalis stimulation causes a depolarization of individual cells (Metherate et al., 1992), resulting in a decrease in slow membrane potential fluctuations (1-5 Hz) associated with Up and Down states and increasing fast membrane potential fluctuations (20-40 Hz). The single neuron effects were also mediated by mAChRs (Metherate et al., 1992), and are likely related to the larger changes seen in the cortical EEG. These results demonstrate that activation or suppression of nucleus basalis acts to dramatically modulate cortical dynamics. Taken together, the attributes of the cholinergic system of the basal forebrain make it an attractive candidate for the dynamic modulation of sensory processing in a behaviorally relevant manner.

1.4 Effects of acetylcholine on stimulus-driven responses of V1

A number of studies have examined the effects of cholinergic activation on sensory-driven responses in visual cortex. Most of these studies used iontophoresis to apply acetylcholine directly to the cells, but in some cases nucleus basalis stimulation was used. What follows is a brief summary of the results.

Cell excitability

Several researchers have noticed changes in the firing rate of cortical cells in response to nucleus basalis stimulation, changes that may affect how the cortex responds to sensory stimuli. The predominant effect on excitatory neurons is facilitatory, though in some cases suppressive effects of acetylcholine application were seen in superficial layers (layer 2/3) (McCormick, 1992). The

excitatory effect on deep layer pyramidal neurons is due to the inactivation of a hyperpolarizing K^+ current by mAChR activation, leading to depolarization and a higher spike rate (McCormick, 1992). The K^+ current is voltage-sensitive and is activated by membrane potential depolarization, likely contributing to the generation of slow cortical oscillations. Another group found that inhibitory interneurons differ in their response to acetylcholine depending on their cell type. Electrophysiologically defined fast-spiking cells were suppressed by acetylcholine application while low-threshold spiking cells were excited (Xiang et al., 1998). These results show that acetylcholine has complex layer and cell type specific effects on cell excitability in visual cortex, which may modulate the processing of visual input.

Functional connectivity

Another notable result of acetylcholine application onto cortex is alteration of the functional connectivity between neurons. In slices containing both thalamus and somatosensory cortex, researchers used whole-cell patch to measure the response of cortical neurons to either thalamic or cortical stimulation (Gil et al., 1997). They found that in the presence of acetylcholine, thalamocortical synapses were strengthened and intracortical synapses were weakened. Another group found that cortical application of acetylcholine to somatosensory cortex increased local field potentials evoked by sensory stimulation but not by intracortical stimulation (Oldford and Castro-Alamancos, 2003); another group found similar results in auditory cortex (Metherate and Ashe, 1993). Finally, voltage-sensitive dye imaging in visual cortical slices has revealed that acetylcholine application suppresses intracortical stimulation in all layers, but only suppresses white matter stimulation in superficial and deep layers, suggesting that the relative strength of thalamocortical inputs would be enhanced relative to intracortical inputs in visual cortex (Kimura et al., 1999). Taken together, these results indicate that acetylcholine alters functional connectivity, and that the functional connectivity may be adjusted as to favor thalamocortical inputs relative to intracortical interactions.

Orientation tuning and direction selectivity

A number of groups have used iontophoresis to apply acetylcholine onto visual cortical neurons while measuring their tuning properties to investigate changes in orientation tuning and direction selectivity. One group investigated this issue by iontophoretically applying acetylcholine onto the visual cortex while recording responses to moving bars (Sato et al., 1987). They found that acetylcholine often decreased the orientation selectivity, though in some cases they found increases. However, another study found no effect of acetylcholine iontophoresis on orientation selectivity (Sillito and Kemp, 1983). The effect of acetylcholine on direction selectivity is also unclear, with studies finding both decreases (Muller and Singer, 1989; Sato et al., 1987) and increases (Sillito and Kemp, 1983) of direction selectivity. These conflicting results could be the result of the method used for applying acetylcholine. Since iontophoresis only affects one or a small number of neurons, and acetylcholine has layer and cell type specific effects, the effect of acetylcholine iontophoresis may depend highly on the location of drug application.

Spatial receptive field structure

The effect of acetylcholine on spatial receptive fields of visual cortical neurons has not been thoroughly researched. One study investigated the effect of acetylcholine on length tuning of cortical neurons to bars of different lengths (Roberts et al., 2005). They found that with acetylcholine application, V1 neurons shifted their tuning towards bars of shorter lengths. However, length tuning may be effected by non-classical elements of the receptive field, so their result might not relate directly to changes in receptive field size or shape. As reported earlier, desynchronized EEG is correlated with smaller receptive fields in visual cortex (Worgotter et al., 1998). Since basal forebrain cholinergic activation desynchronizes the EEG, it might also reduce receptive field size, but direct experimentation is necessary to test this possibility.

Response gain

Another important property of visual cortical neurons with respect to the fidelity of stimulus encoding is the response gain of individual cells to sensory stimuli. One study found an increase in the response gain of layer 4 neurons following iontophoresis of nicotine (Disney et al., 2007). Several more found more widespread increases in the signal-to-noise ratio of cortical responses (Sato et al., 1987; Sillito and Kemp, 1983), but these results were contradicted by a more recent study (Zinke et al., 2006). Once again, these discrepancies might be the result of acetylcholine iontophoresis having different effects in different parts of the cortical circuit.

Attentional modulation and memory

Several groups have found that pairing nucleus basalis stimulation with a stimulus enhances memory and cortical representation of that stimulus (Bakin and Weinberger, 1996; Kilgard and Merzenich, 1998). Also, iontophoresis of acetylcholine onto visual cortical neurons enhances top-down visual attention in monkeys (Herrero et al., 2008). This suggests that, in addition to any role in enhancing overall processing, acetylcholine may also gate memory and top-down forms of selective attention.

1.5 **Summary and motivation**

Sensory processing is actively modulated during periods of wakefulness, arousal, and attention, but it is not understood how this modulation occurs. The primary visual cortex is a useful region for observing the effects of sensory modulation, as the response properties of V1 neurons have been well characterized. The basal forebrain cholinergic system meets the criteria expected of a physiological system capable of dynamically modulating sensory processing on a large scale. Researchers have begun to characterize the effect of acetylcholine on individual cortical neurons. However, these experiments ignore the effects that widespread cholinergic activation might have on cortical dynamics and functional connectivity throughout the cortical circuit (as well as any non-cortical effects of nucleus basalis activation). Thus, in the present study, stimulation of the nucleus basalis will be paired with large-scale recordings of V1 cortical neurons to characterize the effect of basal forebrain activation on sensory processing.

Chapter 2. Cholinergic modulation of V1 cortical state and response properties

2.1 Preface

The first step in determining the effect of basal forebrain activation on visual cortical processing is to characterize the effect on cortical dynamics and single neuron response properties. To this end, I recorded local field potentials (LFP), multi-unit activity, and single neuron activity from area V1 of anesthetized rats using silicon polytrodes while intermittently stimulating nucleus basalis. Here I show that nucleus basalis stimulation markedly alters visual cortical LFP throughout the cortical column, causing a decrease in low frequency LFP activity (1-10 Hz) and an increase in high frequency activity (10-100 Hz), particularly in the gamma band (30-50 Hz); these changes are on the timescale of seconds. Nucleus basalis stimulation also has moderate effects on single neuron response properties. Specifically, while nucleus basalis stimulation does not affect the structure of cortical receptive fields, it improves the signal-to-noise ratio. The influence of nucleus basalis stimulation on orientation tuning and direction selectivity was also investigated, but no clear effects were found. Taken together, these results indicate that nucleus basalis has little effect on the structure of single neuron receptive fields, but has a powerful influence on neuronal gain and cortical dynamics, which likely influences the coding of more complex visual stimuli. Portions of this chapter have been published in the journal *Nature Neuroscience* (Goard and Dan, 2009).

2.2 Methods

Surgery

All experimental procedures were approved by the Animal Care and Use Committee at the University of California, Berkeley. Adult male Long-Evans rats (250–350 g) were anesthetized with urethane (IP, 1.45 g/kg). Animals were restrained in a stereotaxic apparatus (David Kopf Instruments); body temperature was maintained at 37.5° C via a heating pad. Bipolar stimulating electrodes were stereotaxically implanted in the left nucleus basalis, and nucleus basalis was stimulated with trains of 50 pulses (0.1 ms/pulse) at 100 Hz. A craniotomy (diameter ~1 mm) was made either above the monocular region of left V1 or above the left LGN. A small portion of the dura was removed to allow insertion of a silicon polytrode (27 active channels separated by 50 μm, NeuroNexus Technologies). Signals were recorded with the Cheetah 32-channel acquisition system (Neuralynx) at 30 kHz. The right eye was fixed with a metal ring to prevent eye movement and irrigated with sterile saline. Following the experiment, animals were euthanized with an overdose of isoflurane. A total of 49 rats were used in this study.

Histochemistry

For histochemistry experiments, the animal was deeply anesthetized with urethane and immediately perfused with chilled 4% paraformaldehyde (PFA) solution in 0.1 M PBS. The brain was removed and fixed in 4% PFA/PBS solution overnight at 4° C. After fixation, the brain

was sectioned into 150 μm horizontal slices using a vibratome (Serial 1000 Tissue Sectioning System, Ted Pella Inc). For acetylcholinesterase histochemistry, slices were incubated in 4 mM acetylcholine iodide, 4 mM copper sulphate, and 16 mM glycine in a 50 mM sodium acetate solution (pH 5.0) for 15 hr at 23° C and developed in 1% sodium sulphide solution (pH 7.0) for 10 min at 23° C. This procedure was performed in 15 of the 49 experiments included in this study.

Visual stimuli

Visual stimuli were generated with a PC computer containing a NVIDIA GeForce 6600 graphics board and presented with a XENARC 700V LCD monitor (19.7 cm × 12.1 cm, 960 × 600 pixels, 75 Hz refresh rate, 300 cd m^{-2} maximum luminance, gamma corrected with custom software) located 14 cm from the right eye, positioned such that the receptive fields of the recorded neurons were at the center of the monitor.

For layer identification, a 9 x 9 pixel checkerboard was alternated in polarity at 0.5 Hz (eliciting a luminance-independent cortical response). For measuring receptive fields, sparse noise consisting of random flashes of white and black pixels (100% contrast, 4.5^o $pixel^{-1}$, 100 ms per flash) on a gray background was used. For measuring orientation tuning and direction selectivity, drifting gratings (100% contrast, 2 Hz, 0.04 cycles deg^{-1}) were used.

Analyses

Local field potential analysis was carried out using Gabor/Morlet wavelet decomposition (http://dxjones.com/matlab/timefreq/). For single unit isolation, polytrode contact sites (channels) were separated into groups (2–4 channels per group) and spike waveforms were sorted using NeuroScope (http://neuroscope.sourceforge.net), NDManager (http://ndmanager.sourceforge.net), and Klusters (http://klusters.sourceforge.net) (Hazan et al., 2006). In some instances, a single neuron was picked up by more than one electrode group. To ensure that duplicate neurons were not included in the subsequent analyses, pairwise between-neuron correlation coefficients (CC; binned at 1000 Hz) were calculated following clustering; for any pair with CC > 0.1, the cell with lower firing rate was discarded. For the remaining single units, only those with firing rates > 0.5 spikes s^{-1} were included in further analyses, performed in MATLAB (The Mathworks).

To quantify the ON and OFF receptive fields measured with sparse noise, each receptive field was fitted with a two-dimensional Gaussian function:

$$R(x,y) = a_0 + ae^{-\left(\frac{(x-x_0)^2}{2\sigma_M^2}+\frac{(x-x_0)^2}{2\sigma_M^2}\right)}$$

where $R(x,y)$ is the response at pixel position (x,y), a_0 is the DC component, a is the receptive field peak amplitude, (x_0,y_0) is the receptive field center, and σ_M and σ_m are the standard deviations along the major and minor axes. The receptive field size is measured by $\pi\sigma_M\sigma_m$, and the amplitude/baseline ratio is measured by a/a_0.

To measure orientation tuning and direction selectivity, firing rate as a function of orientation was fitted as the sum of two Gaussians with peaks 180˚ apart:

$$R(\theta) = a_0 + a_1 e^{\frac{-(\theta-\theta_0)^2}{2\sigma^2}} + a_2 e^{\frac{-(\theta-\theta_0+180^\circ)^2}{2\sigma^2}}$$

where $R(\theta)$ is the response at orientation θ, a_0 is the DC component, a_1 and a_2 are the amplitudes of the two Gaussians, θ_0 is the preferred orientation, and σ is the standard deviation. Tuning width is measured by σ, and direction selectivity is measured by $[R(\theta_0) - R(\theta_0+180^\circ)] / [R(\theta_0)+ R(\theta_0+180^\circ)]$.

To test statistical significance, Wilcoxon signed-rank test was used for paired samples and Wilcoxon rank-sum test was used for unpaired samples.

2.3 Stimulation of the basal forebrain cholinergic system

In order to investigate the role of basal forebrain stimulation on visual cortical processing, anesthetized rats were implanted with a bipolar stimulating electrode in nucleus basalis and a recording polytrode in region V1 (**Fig. 2.1**).

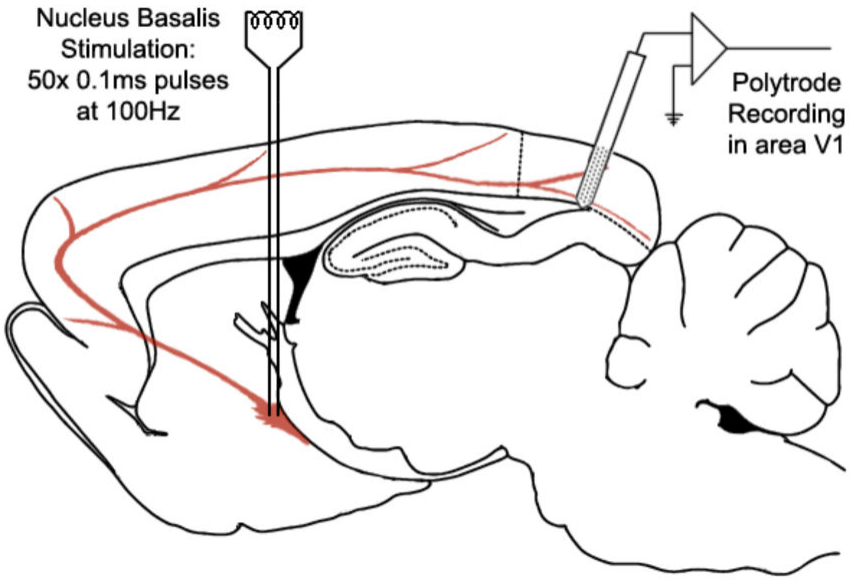

Figure 2.1: Experimental schematic. A bipolar stimulating electrode was placed in the nucleus basalis to activate cortically projecting cholinergic fibers. Cortical activity was recorded from area V1 using a silicon polytrode.

Nucleus basalis was found by slowly lowering the electrode at the appropriate stereotaxic coordinates until stimulation elicited a desynchronization of the cortical EEG, measured from two locations on contralateral sides of the skull (**Fig. 2.2**).

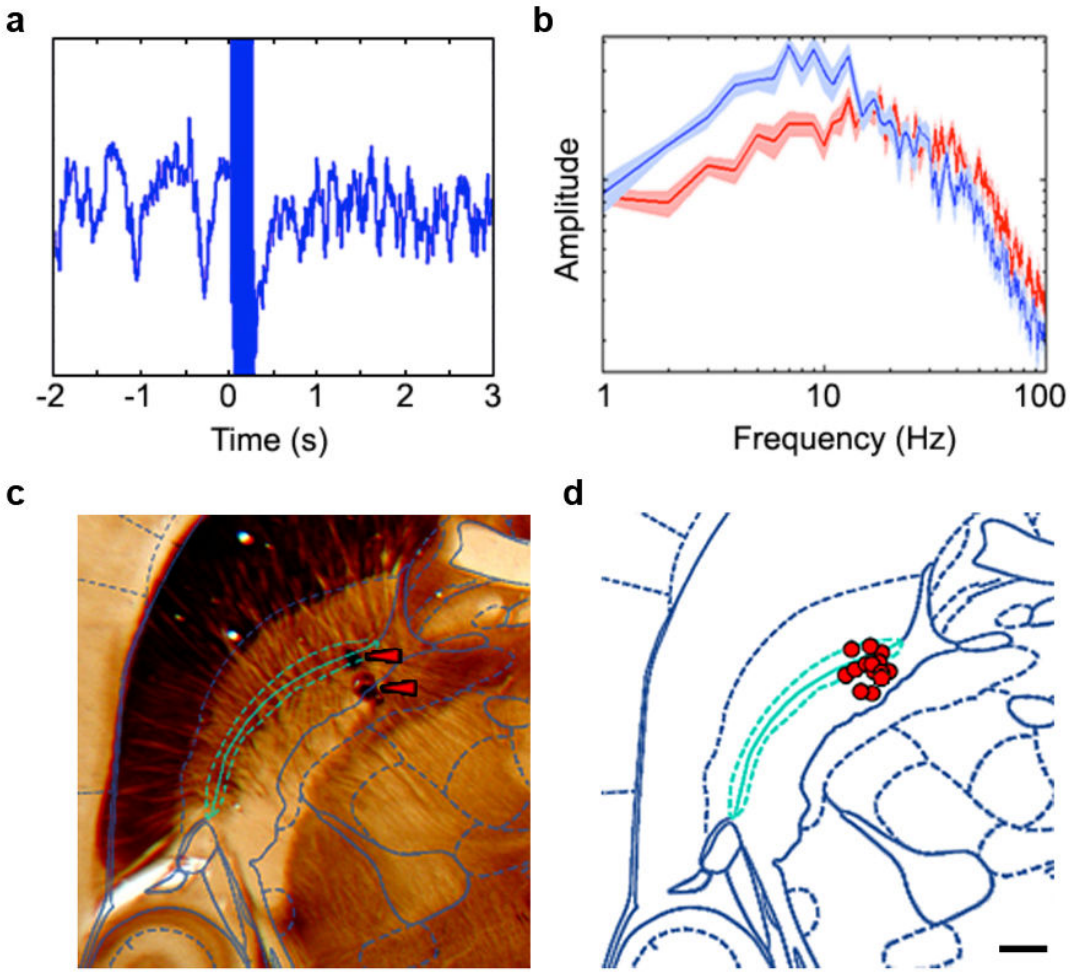

Figure 2.2: Stimulation of nucleus basalis desynchronizes cortical EEG in the anesthetized rat. (a) Example EEG trace before and after nucleus basalis stimulation at $t = 0$. **(b)** Amplitude spectra of EEG 1s before (blue) and 1s after (red) nucleus basalis stimulation, averaged over 15 trials. Shaded area, ± s.e.m. (**c**) An example of stimulation electrode localization using acetylcholinesterase histochemistry. Nucleus basalis is shown in cyan in overlay diagram (Paxinos and Watson, 1998). Red arrowheads, bipolar electrode tracts. (**d**) Summary of electrode positions relative to nucleus basalis (cyan) for 15 experiments. Red circle, centroid of the pair of electrode tracts in each experiment, which was within 300 μm of nucleus basalis for all 15 experiments. Scale bar, 500 μm.

Once desynchronization was observed in the EEG traces (**Fig. 2.2a**), the nucleus was stimulated several times to ensure statistically significant desynchronization. Desynchronization was quantified by averaging the Fourier transform of repeated traces before and after stimulation (**Fig. 2.2b**). The stimulation was considered successful if it resulted in significantly less power in the 1-10 Hz frequency band and significantly more power in the 10-100 Hz frequency band in the two seconds following stimulation.

Nucleus basalis is the only structure in the stimulated region known to elicit cortical desynchronization, but to further ensure that the correct anatomical structure was being activated, acetylcholinesterase histochemistry was performed in a subset of experiments ($n = 15$ out of 49). This stain demarcated the acetylcholinesterase-rich neurons of the nucleus basalis from the surrounding structures, and was fit to a structure overlay from a rat atlas (Paxinos and Watson,

1998) to determine the relative position of the electrode tracts to nucleus basalis (**Fig. 2.2c**). In all 19 experiments in which acetylcholinesterase histochemistry was performed, the centroid of the bipolar electrode was within 300μm of the anatomically defined nucleus basalis (Paxinos and Watson, 1998) (**Fig. 2.2d**).

2.4 Polytrode recording in visual cortex

To record local field potentials, multi-unit activity, and single unit responses from populations of isolated neurons, silicon polytrodes (Blanche et al., 2005) were inserted into the primary visual cortex (**Fig. 2.3**). Polytrodes are high-density silicon electrode arrays that allow recording from a continuous span through the depth of cortex. The electrode sites are evenly spaced at 50μm intervals so that traditional unit triangulation techniques can be used to isolate single neurons (Wilson and McNaughton, 1993). The polytrodes are only 15μm thick, so they cause little damage to the local cortical area (Blanche et al., 2005).

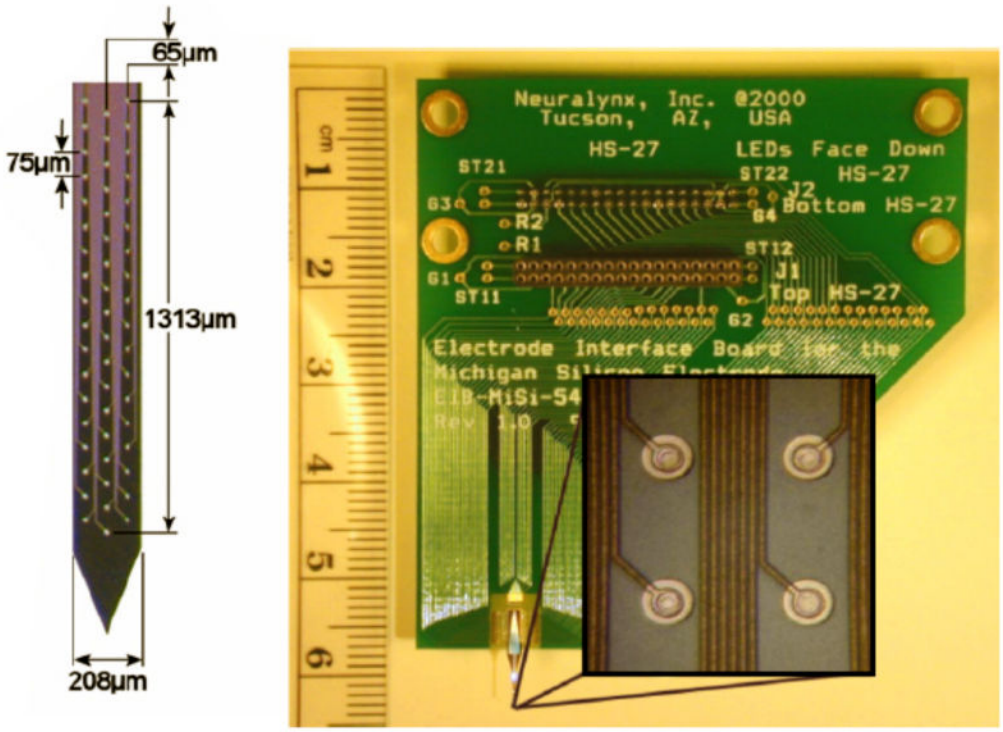

Figure 2.3: Silicon polytrode used for cortical recordings. Adapted from Blanche et al. (2005).

Continuous recordings (30kHz sampling rate) of neural activity were made from 27 channels (two columns of electrode sites) of the polytrode in all experiments. For the recording of LFP, the traces were low pass filtered and directly analyzed for spectral content. For spiking activity, the signal was first high pass filtered (**Fig. 2.4**, middle), then either binned into multi-unit peri-stimulus time histograms (PSTH; **Fig. 2.4**, top) or the signals were sorted to isolate single neurons (**Fig. 2.4**, bottom).

For spike sorting, channels were divided into groups of three to form virtual tritrodes. Spike events were determined using a noise-based threshold (Hazan et al., 2006). After automated clustering, the isolated neurons were manually examined to make sure that they had a clear refractory period (activity within the refractory period is a sign of under-clustering), and no obvious refractory period in the cross correlations with other neurons (a sign of over-clustering). In general, a single polytrode recording was capable of recording from 10-30 well isolated neurons, of which ~75% were visually responsive.

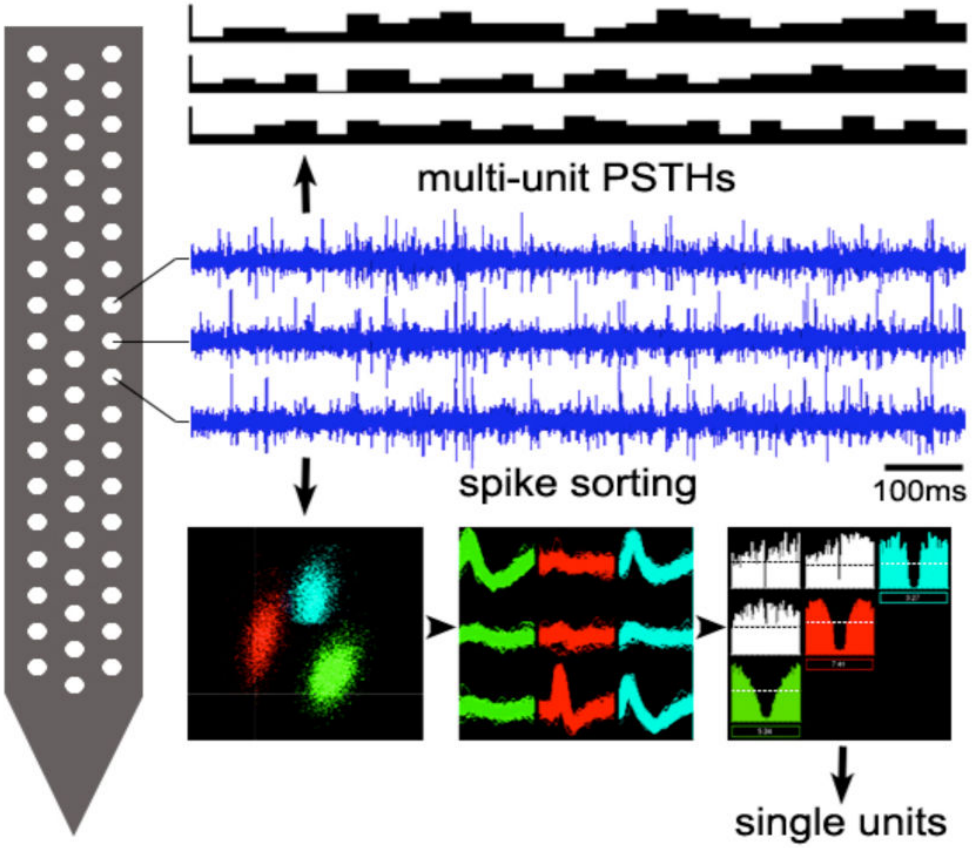

Figure 2.4: Schematic illustrating analysis procedures for continuously acquired signals. High pass filtered signals shown from three channels (blue traces, middle), spike events were determined by noise-based thresholds. For some analyses, multi-unit activity was binned into multi-unit PSTHs (top), in others, single units were isolated using existing spike sorting methods (bottom). The bottom panel shows three cells (red, green, cyan) isolated in PCA space (bottom left), their waveforms (bottom center), and the auto- and cross- correlations used for ensuring appropriate clustering (bottom right). As can be seen, all three cells have clear refractory periods in the auto-correlation (not under-clustered) and no refractory period in the cross-correlation between cells (not over-clustered).

Another advantage of polytrode recording over traditional recording techniques is that the channels are evenly spaced throughout the cortex, allowing reliable determination of the cortical layer corresponding to each polytrode channel (Blanche et al., 2005).

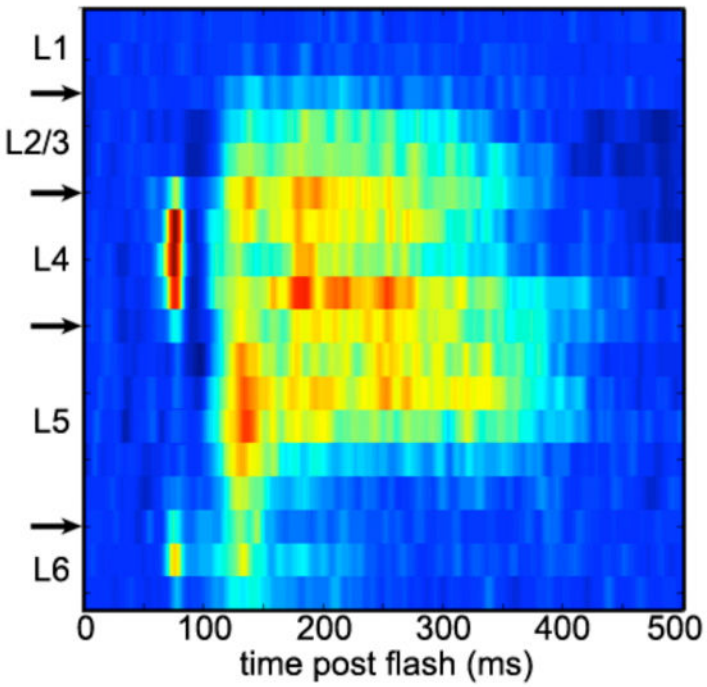

Figure 2.5: Using multi-unit cortical response for identification of cortical layers. Averaged cortical response to alternating checkerboard stimulus. Short latency responses are seen in cortical layers 4 and 6 due to direct thalamocortical input. Slower responses are seen in layers 2/3 and 5.

Traditionally, current source density analysis using LFP recordings is used to determine the location of each layer. However, examining the average multi-unit response to an alternating checkerboard is an equally robust measure, as different layers respond with different latencies to visual stimulation (**Fig. 2.5**; layer 4 and layer 6 respond first, as they receive direct thalamocortical input, and layers 2/3 and 5 respond with longer latency). Using multi-unit spiking avoids the spatial averaging that occurs with LFP measurements. In a subset of experiments, layer assignments determined with the two methods were compared and found to be similar.

2.5 Effect of nucleus basalis stimulation on cortical LFP

As a first step in investigating the effect of basal forebrain activation on V1 cortical dynamics, I measured the effect of stimulation on the cortical LFP in the absence of visual stimulation. Measuring the change in LFP elucidated the effect of nucleus basalis activation on oscillations of various frequencies. It also allowed quantification of the time course of changes in cortical activity mediated by a single stimulation event. The time course recovered from these experiments was then used to determine the appropriate length of visual stimulation in the next series of experiments.

For LFP measurements, continuous signals acquired through the polytrode channels were low pass filtered with a 300 Hz cutoff to eliminate spiking activity and pass lower frequencies. The lowpass filtered LFP activity has been found to reflect the summed dendritic synaptic activity from many neurons within a local area (~250 μm) around the electrode (Katzner et al.,

2009). This measurement is effective at capturing oscillating inputs that in turn reflect the membrane potential fluctuations of local neurons (Poulet and Petersen, 2008). In order to analyze the frequency activity as a function of time after stimulation, I used a wavelet transform to determine the frequency composition of LFP signal. Conceptually, the wavelet decomposition is similar to the power spectrum of a signal, in which the signal is binned into discrete lengths of time, and the frequency content of each bin is determined with a discrete Fourier transform. However, one shortcoming of the analyzing the power spectrum is that oscillations of different frequencies are best analyzed using time bins of different sizes— higher frequency signals tend to be short lasting and can be adequately sampled with small time bins, while lower frequency signals tend to be longer lasting and benefit from additional sampling with large time bins. The wavelet transform addresses this issue by sampling different frequencies with different time bins (using a series of Gabor/Morlet wavelet filters), optimizing the resolution of frequency measurements throughout the spectrum.

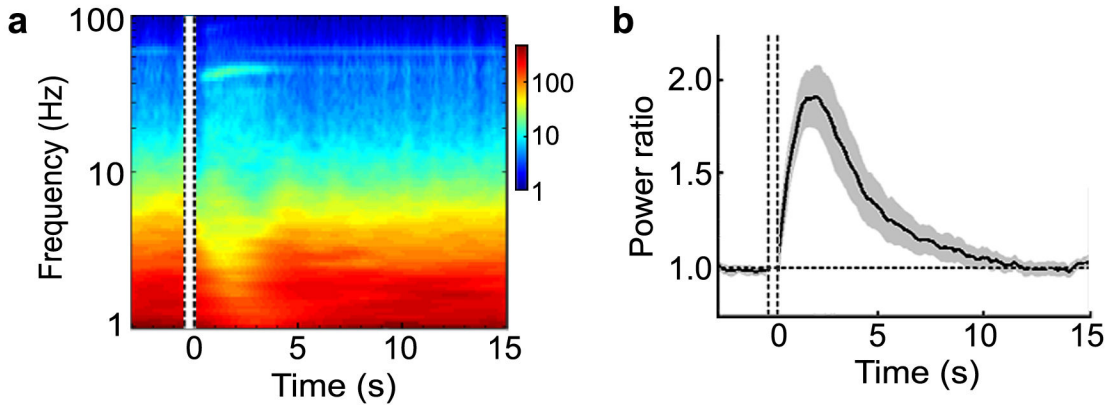

Figure 2.6: Effect of nucleus basalis stimulation on cortical LFP. (a) Wavelet decomposition analysis of LFP before and after nucleus basalis stimulation from an example experiment, averaged over 30 trials. Amplitude is color coded (scale bar on the right, arbitrary unit). Vertical lines, period of nucleus basalis stimulation (500 ms). No visual stimuli were presented. **(b)** Power ratio (LFP power at 10 to 100 Hz divided by LFP power at 1 to 10 Hz) averaged across 27 experiments. In each experiment the ratio was normalized by its mean value before nucleus basalis stimulation. Black line, mean; shaded area, ± s.e.m.

By averaging over multiple trials, I measured the average change in frequency composition following nucleus basalis stimulation (the response was averaged across channels spanning cortex, as there was little difference in the frequency content) (**Fig. 2.6a**). Nucleus basalis stimulation resulted in a robust increase in higher frequency activity (10-100 Hz) and decrease in low frequency activity (1-10 Hz) for several seconds following the stimulation. This general trend is similar to that seen in the cortical EEG following nucleus basalis stimulation. However, in the cortical LFP, there was also a striking band pass increase in the gamma frequency range (30-50 Hz; **Fig. 2.6a**) that was robust across experiments. This selective frequency boost is interesting because local gamma band activity has been found to correlate with the presence of top-down attention, as well as higher response gain to visual inputs.

To quantify the time course of the nucleus basalis stimulation effect, the ratio of high frequency (10-100Hz) power to low frequency (1-10 Hz) power as a function of time after

stimulation was averaged across all experiments (**Fig. 2.6b**). The magnitude of the nucleus basalis-induced shift in cortical dynamics rose over a couple of seconds, recovering on a scale of ~5 seconds, though it took up to 10 seconds to fully recover. This time course was consistent throughout multiple hours of recording (data not shown). This suggested that a stimulus presentation of 5 seconds would be appropriate for investigating the effect of nucleus basalis stimulation on processing of visual inputs.

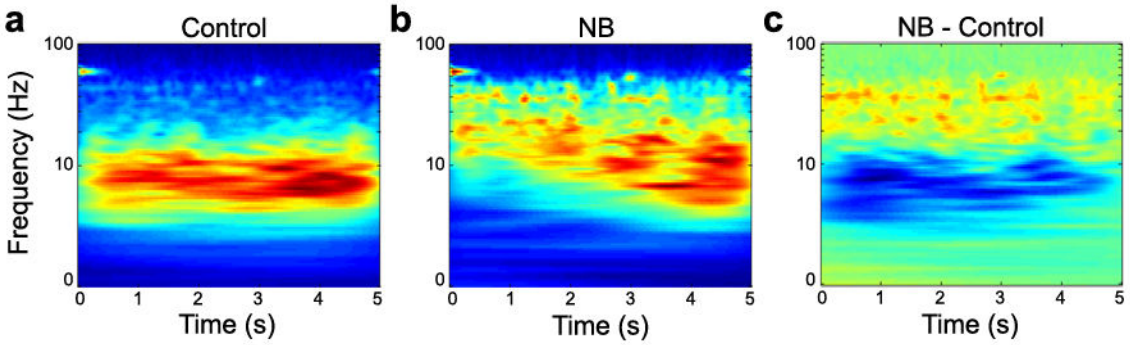

Figure 2.7: Effect of nucleus basalis stimulation on cortical LFP during visual stimulation. (a) Wavelet decomposition analysis of LFP before nucleus basalis stimulation during presentation of a 5 s natural movie. **(b)** Wavelet decomposition analysis of LFP after nucleus basalis stimulation during presentation of a 5 s natural movie. **(c)** Subtraction of decomposition before nucleus basalis stimulation from the decomposition after nucleus basalis stimulation.

To ensure that the time course of the nucleus basalis effect on cortical dynamics was similar with visual stimulation, I calculated the wavelet decomposition of the LFP in response to repeated presentations of a 5 second natural movie (**Fig. 2.7**). The frequency composition of the LFP was similarly affected by the nucleus basalis stimulation throughout the stimulus presentation, with a decrease in lower frequencies and an increase in higher frequencies (**Fig. 2.7c**). Interestingly, the increase in gamma frequency activity was present but less temporally continuous than in the absence of visual stimulation, perhaps due to modulation of the gamma band activity by the natural movies.

2.6 Effect of nucleus basalis stimulation on V1 spatial receptive fields

The next step in characterizing the effect of nucleus basalis activation on cortical processing was to investigate its effects on single neuron response properties. No attempt has been made to measure the effect of nucleus basalis stimulation on spatial receptive fields, but previous findings (see Chapter 1.4) suggest that EEG desynchronization might affect the receptive field size.

To measure the receptive fields of V1 cortical neurons, the animals were presented with sparse noise stimulation to the contralateral eye (Jones and Palmer, 1987). Each frame of the sparse noise stimulation consisted of a grey background with a single white or black pixel 4.5° on a side. The ON (OFF) receptive field was measured by averaging together each frame containing a white (black) pixel, multiplied by the number of spikes it elicited (**Fig. 2.8a**). This produced a map of the optimal ON and OFF stimuli for each neuron (**Fig. 2.8b**). Sparse noise has the advantage over white noise that neurons with overlapping ON and OFF receptive fields can still be mapped (with white noise, the overlapping responses would average out and the response

would be lost). This allows measurement of spatial receptive fields for V1 complex cells as well as simple cells.

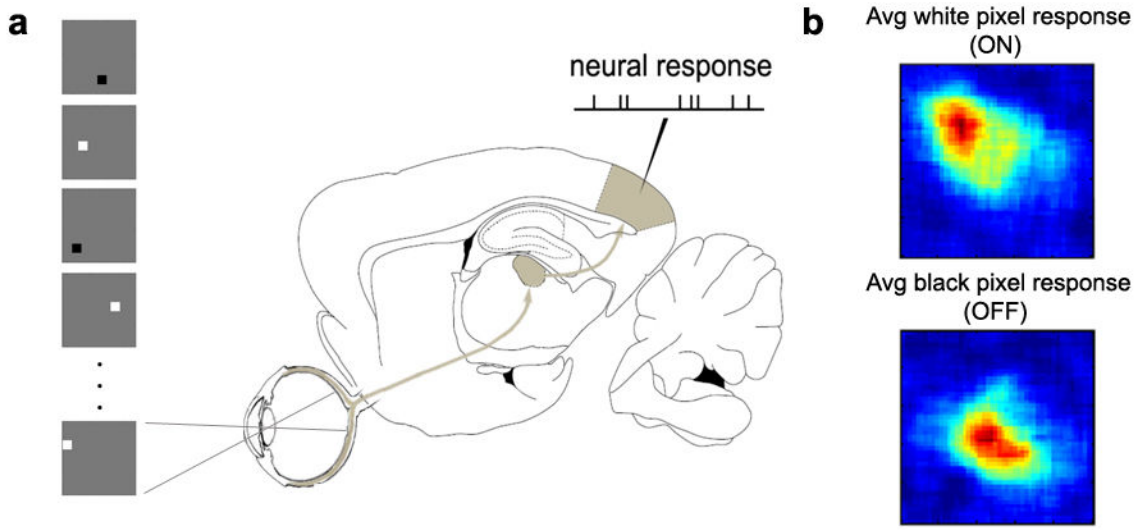

Figure 2.8: Measuring of V1 spatial receptive fields using sparse noise. (a) Sparse noise frames with either white or black squares on a grey background (randomly interleaved) were presented at 10Hz to the contralateral eye. **(b)** Example receptive fields from a cortical neuron: (top) ON receptive field constructed by averaging white pixel responses, (bottom) OFF receptive field constructed by averaging black pixel responses. Color scale same as Fig. 2.9b.

To measure the effect of nucleus basalis stimulation on the spatial receptive fields, 5 s segments of sparse noise stimulation (50 frames) were presented to the animal while nucleus basalis was stimulated on interleaved trials. I quantified the structure of the receptive fields by fitting them with two-dimensional Gaussians (see Methods). As can be seen for two example neurons (**Fig. 2.9a,b**), nucleus basalis stimulation did not have any significant effect on receptive field structure. I found no significant change in receptive field size [$P = 0.07$ (ON) and $P = 0.41$ (OFF), $n = 38$ neurons from 5 experiments, **Fig. 2.9c**]. Nor were there changes in position, aspect ratio, subfield overlap, or any other structural receptive field properties examined (data not shown).

However, as can be seen for the example receptive neurons, both ON and OFF receptive fields showed an increased response within the receptive field, and a decreased response outside of the receptive field. This resulted in a significant increase in the signal-to-noise ratio (measured as the ratio of peak amplitude to baseline; see Methods) for both ON and OFF receptive fields across the population [$P < 10^{-4}$ (ON) and $P < 10^{-4}$ (OFF), $n = 38$ neurons from 5 experiments, **Fig. 2.9d**]. The increase in the neural response gain to sensory inputs could substantially impact the coding of more complex sensory inputs.

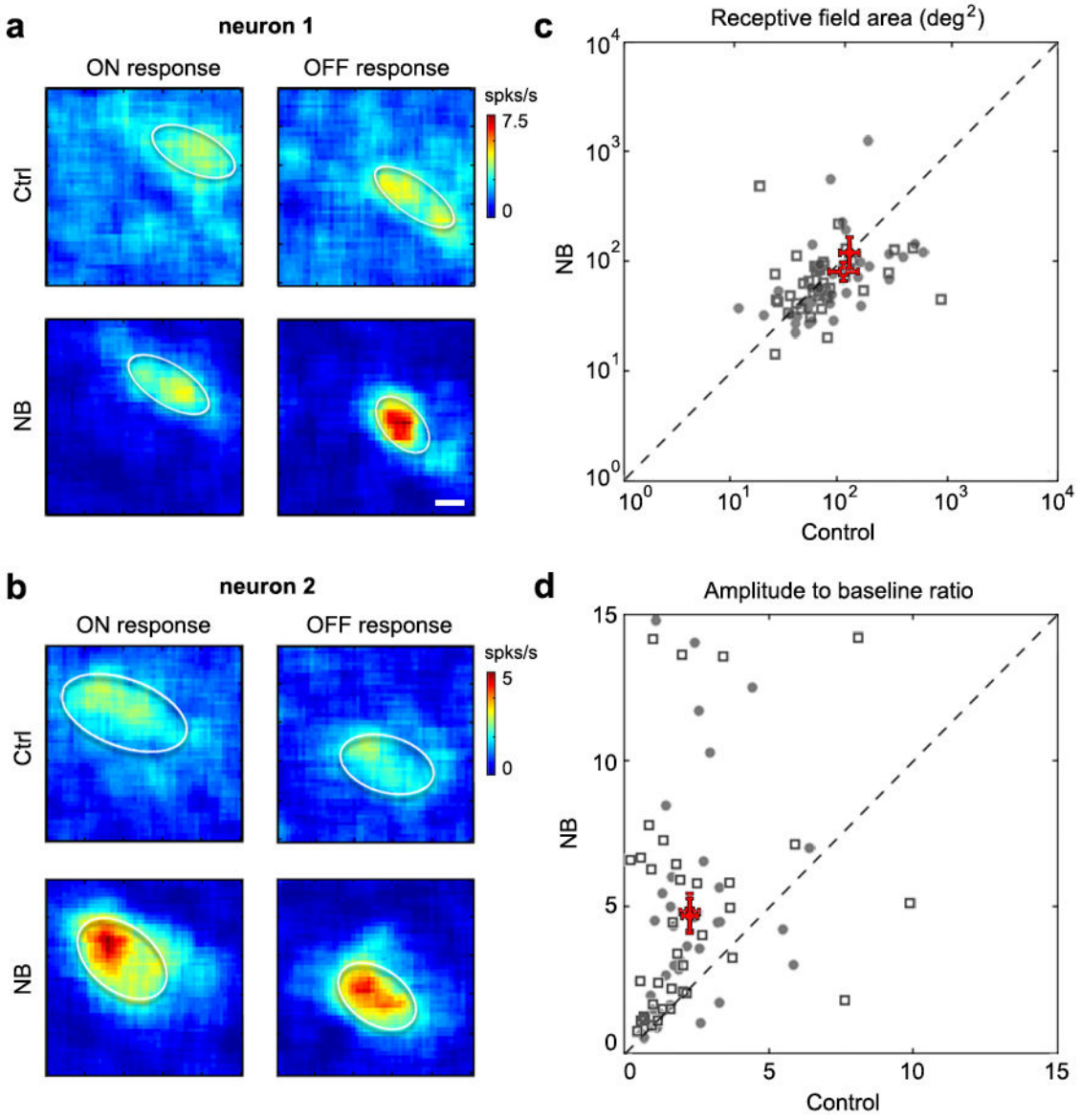

Figure 2.9: Effect of nucleus basalis stimulation on receptive fields of V1 neurons. (a) ON (left) and OFF (right) spatial receptive fields of a V1 neuron before (ctrl, top) and after (NB, bottom) nucleus basalis stimulation. White ellipse, contour of Gaussian fit of the receptive field at one standard deviation along the major and minor axes. Scale bar, 5˚ of visual field. **(b)** ON and OFF receptive fields of a second neuron. **(c)** Summary of receptive field area before and after nucleus basalis stimulation. Each symbol represents the receptive field of one cell (●, ON; □, OFF). **(d)** Amplitude to baseline ratio before and after nucleus basalis stimulation. Error bars, ± s.e.m.

2.7 Effect of nucleus basalis stimulation on orientation tuning and direction selectivity

To further characterize the effect of nucleus basalis stimulation on V1 single cell response properties, I measured the orientation tuning and direction selectivity of isolated neurons. Previous studies showed that cortical iontophoresis of ACh could induce changes in orientation tuning and direction selectivity, although the observed effects were variable between cells and

across studies (see Chapter 1.4). Using drifting gratings to measure the orientation tuning of cortical neurons before and after nucleus basalis stimulation (**Fig. 2.10a,b**), I found no significant change in orientation tuning width (P = 0.78, n = 35 neurons from 10 experiments, **Fig. 2.10c**) or direction selectivity (P = 0.20, n = 35 neurons from 10 experiments, **Fig. 10d**) at the population level.

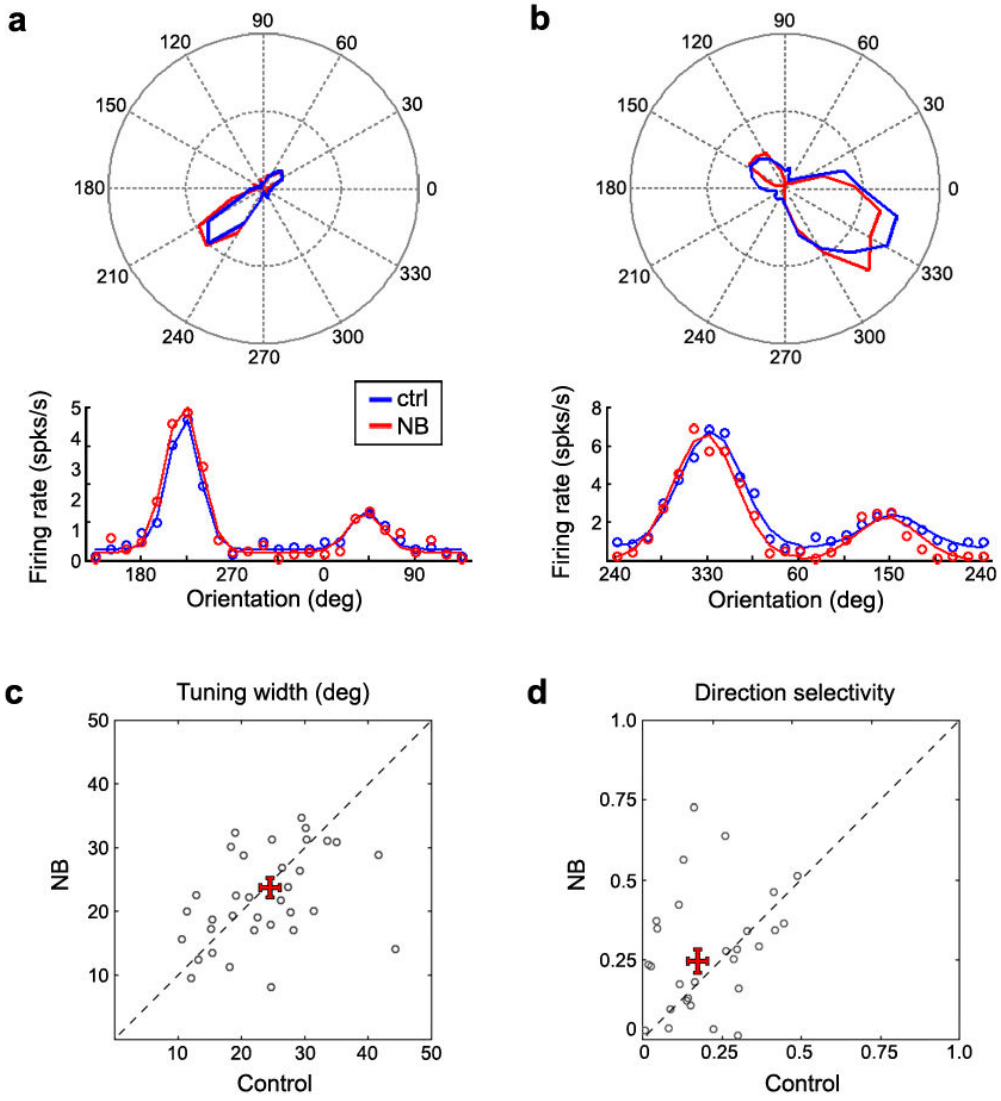

Figure 2.10: Effect of nucleus basalis stimulation on orientation tuning and direction selectivity. (a) Example V1 neuron showing orientation tuning and direction selectivity before (blue) and after (red) nucleus basalis stimulation, plotted on polar (top) and Cartesian (bottom) coordinates. Cartesian plot shows raw data (circles) and Gaussian fit (line). **(b)** Orientation tuning and direction selectivity of a second V1 neuron. **(c)** Orientation tuning width before and after nucleus basalis stimulation. Each symbol represents data from one cell. **(d)** Direction selectivity before and after nucleus basalis stimulation. Nucleus basalis stimulation did not significantly change the tuning width or direction selectivity. Error bars, ± s.e.m.

2.8 Summary

In the current study, the role of the basal forebrain cholinergic system on visual cortical processing was investigated by implanting a bipolar stimulating electrode in nucleus basalis and a silicon polytrode in V1. Stimulating nucleus basalis has a profound effect on cortical dynamics on the time scale of seconds, as reflected by changes in the cortical LFP. Nucleus basalis stimulation does not change the structure of the spatial receptive field, though it does enhance the signal-to-noise ratio of responses to noise stimuli. Furthermore, nucleus basalis stimulation has no consistent effect on the orientation tuning or direction selectivity of cortical neurons. Taken together, these results show that nucleus basalis does not systematically alter the receptive fields of V1 neurons, but rather serves to increase neuronal gain and alter the frequency composition of ongoing cortical dynamics. These effects could have substantial ramifications for the population coding of more complex natural stimuli.

Chapter 3. Basal forebrain activation enhances cortical coding of natural scenes

3.1 Preface

The effect of basal forebrain activation on neuronal gain and cortical dynamics suggests that basal forebrain activity may modulate the encoding of natural sensory stimuli. To analyze the effect of basal forebrain activation on cortical coding, I recorded visual responses to natural movies in V1 while intermittently stimulating nucleus basalis. Here I show that nucleus basalis stimulation acts to decorrelate the responses of V1 neurons while simultaneously improving single-neuron response reliability. Pharmacology experiments showed that the observed decorrelation is dependent on mAChRs, but that the improved reliability does not depend on cortical AChRs. This suggested that the nucleus basalis-induced improvement of reliability occurred further upstream in the visual pathway. Recordings in LGN revealed that thalamic relay neurons also improve in reliability following nucleus basalis stimulation, showing that nucleus basalis stimulation acts in a distributed manner along the sensory pathway. A discrimination analysis showed that nucleus basalis stimulation improves coding of natural scenes, and that the improvement in coding is due to modulation both of single neurons and between-neuron interactions. Thus, the nucleus basalis projection acts to dynamically modulate cortical coding of natural sensory stimuli. Portions of this chapter have been published in the journal *Nature Neuroscience* (Goard and Dan, 2009).

3.2 Methods

Surgery

All experimental procedures were approved by the Animal Care and Use Committee at the University of California, Berkeley. Adult male Long-Evans rats (250–350 g) were anesthetized with urethane (i.p., 1.45 g kg^{-1}). Animals were restrained in a stereotaxic apparatus (David Kopf Instruments); body temperature was maintained at 37.5° C via a heating pad. Bipolar stimulating electrodes were stereotaxically implanted in the left nucleus basalis, and nucleus basalis was stimulated with trains of 50 pulses (0.1 ms $pulse^{-1}$) at 100 Hz. A craniotomy (diameter ~1 mm) was made either above the monocular region of left V1 or above the left LGN. A small portion of the dura was removed to allow insertion of a silicon polytrode (27 active channels separated by 50 μm, NeuroNexus Technologies). Signals were recorded with the Cheetah 32-channel acquisition system (Neuralynx) at 30 kHz. The right eye was fixed with a metal ring to prevent eye movement and irrigated with sterile saline. Following the experiment, animals were euthanized with an overdose of isoflurane. A total of 49 rats were used in this study.

Pharmacology

For topical drug application, a microwell was made by gluing a plastic ring to the skull surrounding the craniotomy. During application, antagonists to mAChRs (atropine, 1 mM) or nAChR (mecamylamine, 1–10 mM) were loaded into the microwell 15 min prior to recording.

For intracortical injection, a glass micropipette (tip size ~10 μm) was fixed to the front of the polytrode such that the tip was close to the center of the polytrode recording sites (layer 4 or 5). Pharmacological antagonists to mAChRs (atropine, 100 μM) or nAChRs (mecamylamine, 100 μM – 1 mM; DHβE, 100 μM) were injected at a rate of 15 nl min^{-1} using a Hamilton syringe and a syringe pump, starting 15 min prior to and continuing throughout the recording period (total volume ~500 nl). Topical and intracortical pharmacology experiments were combined, since results were very similar for both methods.

To block LGN nAChRs and mAChRs (**Fig. 3.12** and **Fig. 3.13**), a mixture of 100 μM atropine and 100 μM mecamylamine was injected at 15 nl min^{-1} starting 15 min prior to and continuing throughout the recording. The volume of injection (~500 nl) was determined in pilot experiments using dye injections to achieve coverage of most of the LGN without going much beyond its borders. To further ensure that the LGN neurons projecting to the recorded region of V1 were well exposed to the antagonists, I bonded a tungsten electrode to the injection pipette and mapped the LGN multiunit receptive field as closely as possible to the V1 multiunit receptive field.

Visual stimuli

Visual stimuli were generated with a PC computer containing a NVIDIA GeForce 6600 graphics board and presented with a XENARC 700V LCD monitor (19.7 cm × 12.1 cm, 960 × 600 pixels, 75 Hz refresh rate, 300 cd m^{-2} maximum luminance, gamma corrected with custom software) located 14 cm from the right eye, positioned such that the receptive fields of the recorded neurons were at the center of the monitor. For natural stimuli, three 5 s clips were selected from the van Hateren natural movie database (van Hateren and Ruderman, 1998). Each image (64 × 64 pixels, 36º × 36º, mean contrast 43%) was updated every 3 refresh frames, corresponding to an effective frame rate of 25 Hz. To avoid onset and offset transients, the first frame was displayed for 1 s prior to the movie and the last frame was displayed for 1 s following the movie.

Each experiment consisted of 6 blocks, and each block consisted of 5 repeats of the three movies under control and 5 repeats under nucleus basalis conditions (**Fig. 3.8**). Under the control condition, the movies were repeated 5 times with 2 s of static image before each movie. Under the nucleus basalis condition, the movies were repeated 5 times as in the control condition, and nucleus basalis stimulation was administered from 1000 ms to 500 ms prior to the start of each movie. To ensure that the effect of nucleus basalis stimulation had diminished before the start of control trials, a blank frame was shown for 30 s following each block. Each experiment thus consisted of 30 movie repeats under control and 30 repeats under nucleus basalis conditions. In blocks 1 to 3, the control repeats preceded the nucleus basalis repeats; in blocks 4 to 6, the sequence was reversed to further eliminate the potential effect of stimulus history on cortical responses.

Analyses

For single unit isolation, polytrode contact sites (channels) were separated into groups (2–4 channels per group) and spike waveforms were sorted using NeuroScope (http://neuroscope.sourceforge.net), NDManager (http://ndmanager.sourceforge.net), and Klusters (http://klusters.sourceforge.net) (Hazan et al., 2006). In some instances, a single neuron

was picked up by more than one electrode group. To ensure that duplicate neurons were not included in the subsequent analyses, pairwise between-neuron correlation coefficients (CC; binned at 1000 Hz) were calculated following clustering; for any pair with CC > 0.1, the cell with lower firing rate was discarded. For the remaining single units, only those with firing rates > 0.5 spikes s^{-1} were included in further analyses, performed in MATLAB (The Mathworks).

For calculation of between-cell and between-trial CC (**Figs. 3.3** and **3.4**), firing rates were binned at 10 Hz (although results were similar for binning from 5 Hz to 25 Hz). To determine whether a given cell was visually driven, I compared the average between-trial CC within movies and between movies. Only cells that had significantly higher within-movie CC (threshold $\alpha = 0.01$, Wilcoxon signed-rank test) were included in further analyses. The burst-tonic ratio was calculated by measuring the number of burst spikes (two or more spikes occurring with ISI < 4 ms following an absence of spiking for > 100 ms) relative to the number of tonic spikes (all spikes not meeting the burst criteria).

For the discrimination analysis (**Fig. 3.14** and **Fig. 3.15**), the responses were also binned at 10 Hz. For each discrimination, the single-trial response in a given bin (A_i, where i is the trial number) was compared to the mean responses (averaged across trials) in the same bin ($<A>$) and in a different bin ($<B>$) based on the Euclidian distances $d(A_i, <A>)$ and $d(A_i, <B>)$. The classification was considered correct if $d(A_i, <A>) < d(A_i, <B>)$, and incorrect if $d(A_i, <A>) > d(A_i, <B>)$. Discrimination performance was assessed by the percentage of correct classifications for all the trials. Since the discrimination performance is expected to increase nonlinearly with the number of neurons, it is difficult to measure the redundancy between neurons. I thus converted the discrimination performance into a measure of information as $I = 1 + (p)\log_2(p) + (1-p)\log_2(1-p))$, where p is the discrimination performance (note that when discrimination is at chance level, $p = 50\%$, $I = 0$). This definition of I represents the mutual information between the actual stimulus and the stimulus decoded from the neuronal response by the 'ideal observer' in the discrimination analysis. $I(N)$ is computed as the average information across all combinations of N simultaneously recorded cells in each experiment, and it should increase linearly with N if there is no redundancy between neurons. Downward deviation from the diagonal line in **Fig. 3.15c** thus reflects the degree of redundancy. For population analyses (**Fig. 3.15a,c**), only experiments with ≥ 15 simultaneously recorded single units were included (12/19 experiments).

To test statistical significance, Wilcoxon signed-rank test was used for paired samples and Wilcoxon rank-sum test was used for unpaired samples; multiple comparisons were corrected with the Bonferroni method.

3.3 Nucleus basalis stimulation decorrelates visual responses and improves single neuron reliability

To investigate the effect of nucleus basalis on cortical coding of natural visual scenes, 5 s clips of natural movies were displayed to the contralateral eye while nucleus basalis was stimulated intermittently.

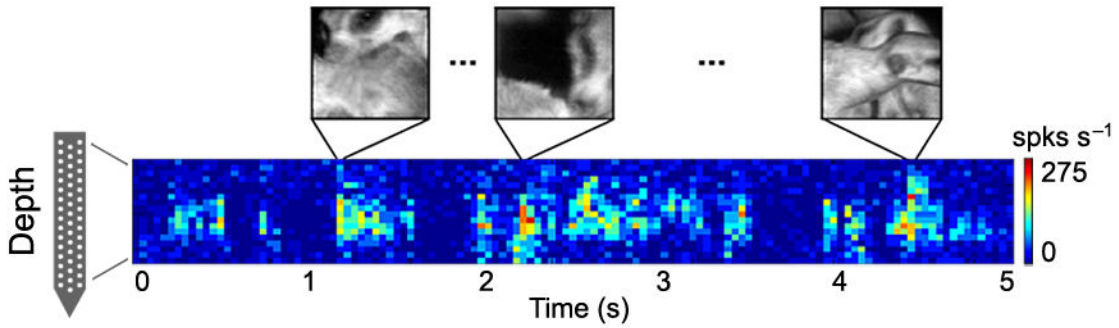

Figure 3.1: Measuring responses to natural movie through depth of cortex. Multiunit spike rate (color coded, scale bar on the right) recorded by the polytrode plotted against cortical depth and time during one repeat of a natural movie.

For qualitatively comparing control responses to nucleus basalis responses, multi-unit activity was measured through the depth of cortex while presenting a 5 s natural movie (**Fig. 3.1**). Movies were interleaved, but each was shown a total of 30 presentations in each condition, in order to allow comparison of responses across repeats (see Methods for details). Comparing multi-unit responses to the same movie in control and nucleus basalis stimulation conditions reveals striking differences in multi-unit activity following stimulation (**Fig. 3.2**).

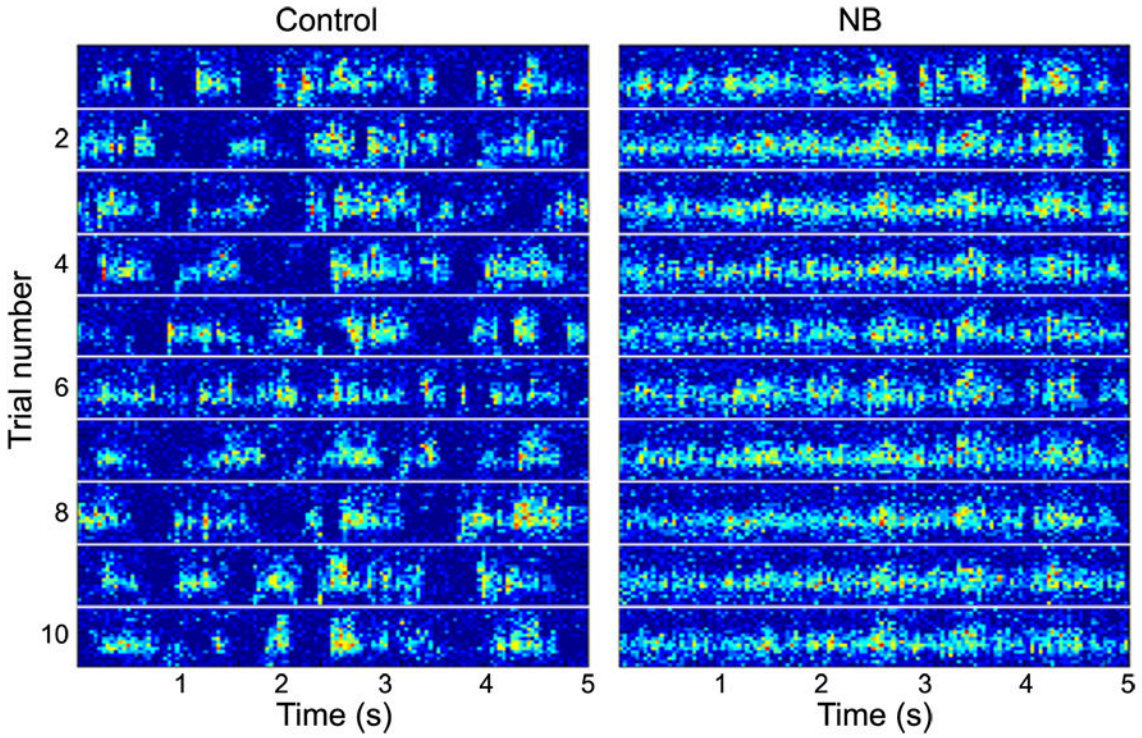

Figure 3.2: Nucleus basalis stimulation modulates multi-unit responses to natural movies. Multiunit responses to the first 10 repeats (trials) of the movie, in the absence of nucleus basalis stimulation (control) or 0 to 5 s after nucleus basalis stimulation (NB), both plotted on the color scale shown in Fig. 3.1.

The most obvious effect of nucleus basalis stimulation on the multi-unit response was a desynchronization of activity across channels. In the control condition, the channels tend to be simultaneously active or silent, while in the nucleus basalis condition the channels are active in a much more independent fashion, such that there is some activity throughout the movie presentation. This suggests that nucleus basalis stimulation might act to decorrelate the population of neurons responding to a stimulus.

In order to investigate this possibility at the level of single neurons, responses of isolated neurons, sorted by depth, to a single movie repeat were compared in the control and nucleus basalis conditions (**Fig. 3.3a**, each neuron indicated by a different color). To quantify the decorrelation for each cell, I computed the average Pearson correlation coefficient (CC) between its response and the responses of all other cells in the same recording. I found that nucleus basalis stimulation caused a strong reduction of between-cell CC across 166 neurons from 19 experiments (**Fig. 3.3b**; $P < 10^{-28}$, Wilcoxon signed-rank test).

The decorrelation of neural responses after nucleus basalis stimulation has ramifications for the coding of natural stimuli. According to information theory, the information transmitted across a channel is maximized when the bits are independent (i.e., the entropy is maximized). More intuitively, if a population of neurons are always concurrently active or silent, the information carried by any one cell is redundant with the other cells in the population— while if the neurons fire independently, they could potentially convey more information about the stimulus. However, independent neural responses would only enhance coding if each independent response carried relevant information about the stimulus. For example, if nucleus basalis stimulation caused the neurons to fire randomly, this would result in decorrelation but not in improved coding of sensory stimuli.

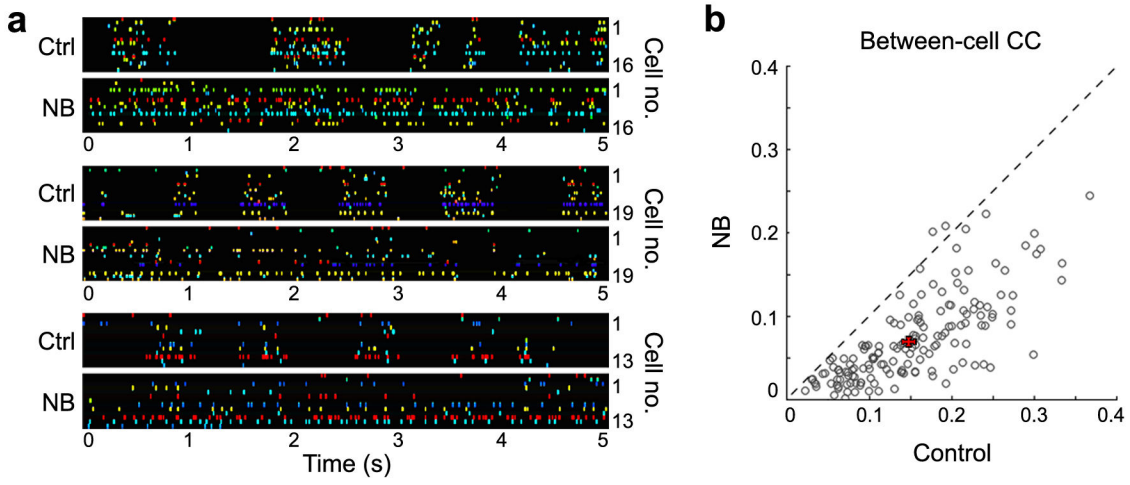

Figure 3.3: Nucleus basalis stimulation decreases correlation between cortical neurons during visual stimulation. (a) Three example experiments illustrating changes in between-cell correlation before (Ctrl) and after (NB) basal forebrain activation. Each panel shows the responses of multiple single units recorded simultaneously during a single movie repeat. Different neurons are indicated by different colors and ordered by cortical depth. **(b)** Summary of between-cell CC before and after nucleus basalis stimulation (n = 166 cells from 19 experiments). Each circle represents the average CC between a single neuron and all other neurons in the same recording. Error bars, ± s.e.m.

Neural responses that carry useful information about the movie will be time-locked to the stimulus presentation. Thus, the effect of stimulation on the coding fidelity of single neurons can be analyzed by measuring the reliability of single neuron responses. To test whether nucleus basalis stimulation had any effect on the single neuron reliability, responses to multiple repeats of a natural movie were compared between conditions (**Fig. 3.4a**, each neuron indicated by a different color). In the control condition, there was considerable variability across trials, but nucleus basalis stimulation markedly improved the reliability of the responses. To quantify the reliability for each cell, I computed the Pearson CC of its responses between each pair of repeats and averaged the CCs over all pairwise combinations. Across the 166 neurons recorded in 19 experiments, nucleus basalis stimulation consistently increased the response reliability (**Fig. 3.4b;** $P < 10^{-28}$, Wilcoxon signed-rank test).

Note that in the experiments in which electrical stimulation of nucleus basalis did not elicit significant desynchronization of cortical EEG ($n = 4$, excluded from the above analyses), neither decreased correlation nor increased reliability was observed (**Fig. 3.5**), suggesting that these effects rely on activation of the same set of neurons that are also responsible for EEG desynchronization.

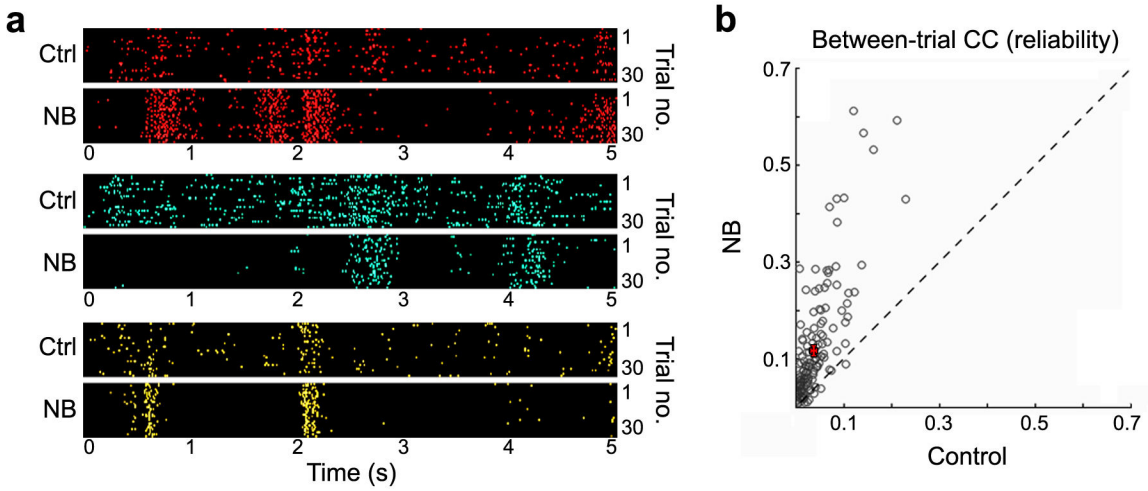

Figure 3.4: Nucleus basalis stimulation increases reliability of individual neurons in response to natural scenes. (a) Three example neurons (indicated by different colors) illustrating changes in response reliability before (Ctrl) and after (NB) basal forebrain activation. Each panel shows the responses of a single neuron to 30 repeats (trials) of a movie. **(b)** Summary of response reliability measured by between-trial CC before and after nucleus basalis stimulation (166 cells from 19 experiments). Each circle represents data from one neuron, averaged over CCs for all pairwise combinations of the 30 trials. Error bars, ± s.e.m.

Effect of electrical stimulation on multiunit activity for experiments with and without EEG desynchronization		
	ΔCC (between-channel)	ΔCC (between-trial)
EEG desynchronization present (mean ± SEM)	-0.16 ± 0.02	0.08 ± 0.01
EEG desynchronization absent (mean ± SEM)	-0.04 ± 0.03	0.02 ± 0.01

Figure 3.5: Effect of electrical stimulation on multiunit activity for experiments with and without significant EEG desynchronization. Experiments with significant EEG desynchronization (n = 19 experiments) showed a significant decrease in between-channel CC ($P < 10^{-7}$) and a significant increase in between-trial CC ($P < 10^{-8}$). Experiments without significant EEG desynchronization (n = 4 experiments) did not show a significant change in either between-channel CC or between-trial CC ($P = 0.31$ and $P = 0.26$, respectively).

When the above analyses were performed for each cortical layer separately, I observed significant decreases in between-cell correlation and increases in response reliability in all layers (**Fig 3.6a,b**). In contrast, the effect of nucleus basalis stimulation on cortical firing rate varied across layers (**Fig 3.6c**): Nucleus basalis stimulation increased the firing rates in layer 4 (133%, $P = 0.10$, Wilcoxon signed-rank test), layer 5 (135%, $P < 10^{-6}$) and layer 6 (126%, $P = 0.13$), but decreased the rate in layer 2/3 (76%, $P = 0.004$).

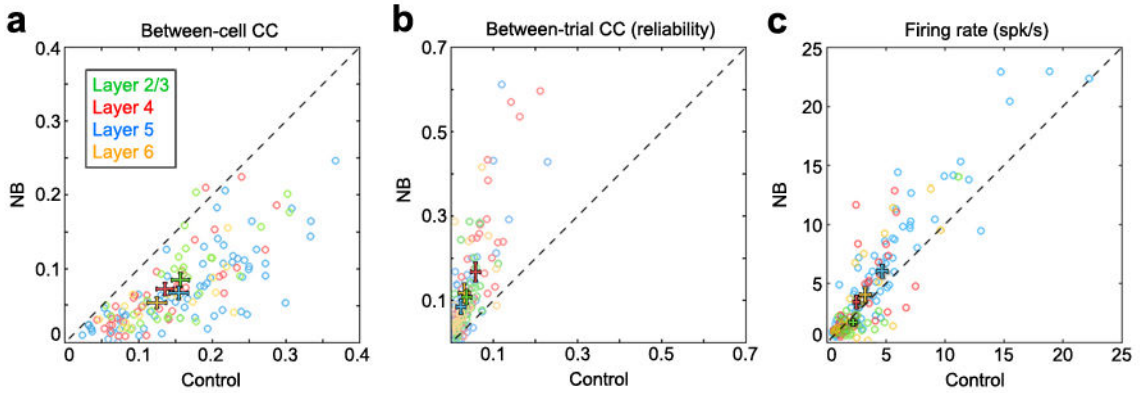

Figure 3.6: Effect of nucleus basalis stimulation on between-cell CC, between-trial CC, and firing rate in each cortical layer. (a) Between-cell CC before and after nucleus basalis stimulation for neurons in layer 2/3 (green, n = 30 neurons), layer 4 (red, n = 40 neurons), layer 5 (blue, n = 77 neurons), and layer 6 (orange, n = 19 neurons), from 19 experiments. The effect was statistically significant for each layer ($P < 0.001$, Wilcoxon sign-rank test). **(b)** Between-trial CC (response reliability) before and after nucleus basalis stimulation for neurons in each layer. The effect was statistically significant for each layer ($P < 0.001$, Wilcoxon sign-rank test). **(c)** Firing rates before and after nucleus basalis stimulation for neurons in each layer. Error bars, ± s.e.m.

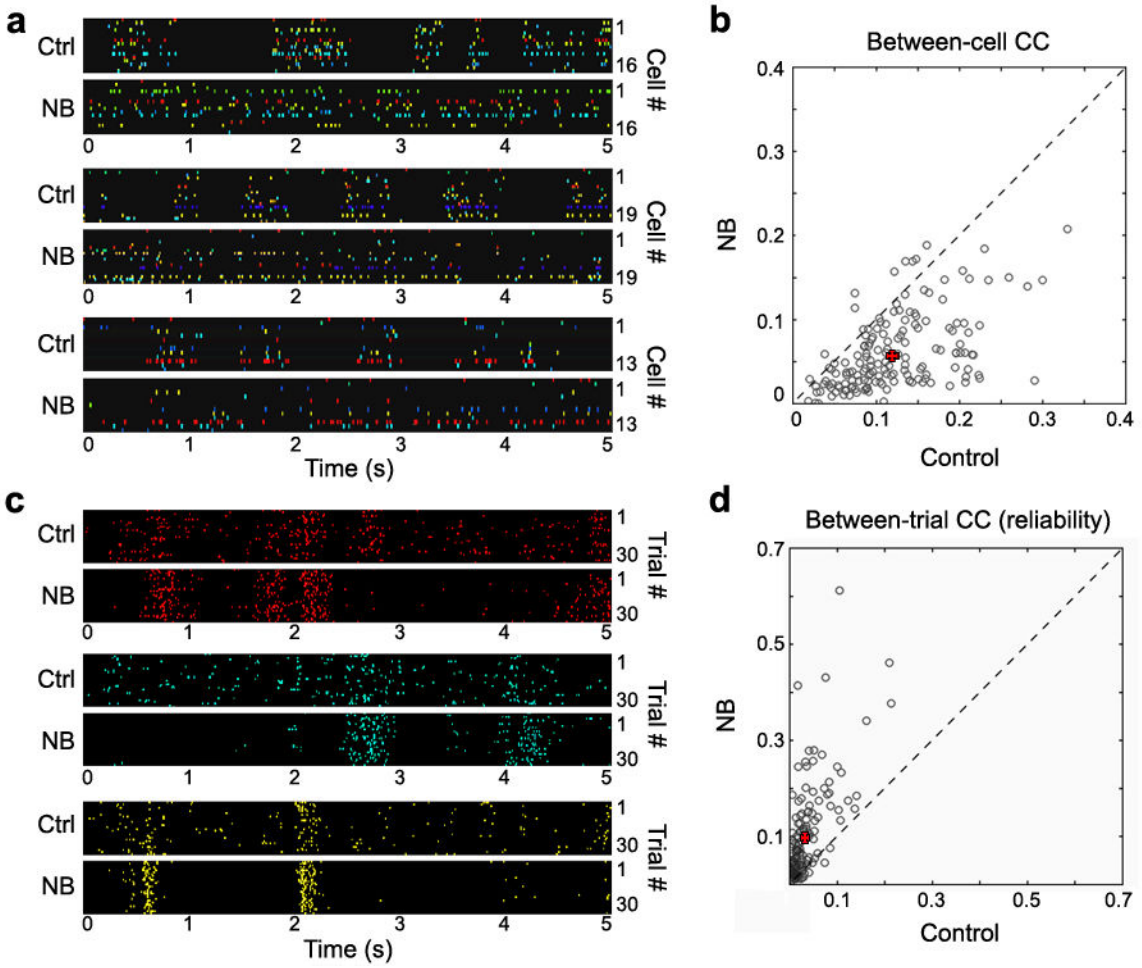

Figure 3.7: Effects of nucleus basalis stimulation on between-cell and between-trial CCs were not due to changes in firing rate. (a) Example experiments shown after the firing rates were equalized before and after nucleus basalis stimulation by randomly removing spikes from the spike train with higher firing rate (same experiments as **Fig. 3.3a**). **(b)** Between-cell CC before and after nucleus basalis stimulation after spike rate equalization. The nucleus basalis-induced decrease in CC remained highly significant. **(c)** Example neurons shown after firing rate equalization (same neurons as **Fig. 3.4a**). **(d)** Between-trial CC before and after nucleus basalis stimulation after spike rate equalization. The nucleus basalis-induced increase in CC remained highly significant. Error bars, ± s.e.m.

To ensure that the changes in between-cell correlation and response reliability were not due to nucleus basalis-induced changes in cortical firing rate, I equalized the firing rates of each neuron before and after nucleus basalis stimulation by randomly deleting spikes from the spike train with higher rate (**Fig. 3.7a**,). Both effects remained highly significant after spike rate equalization (**Fig. 3.7b**,**d** online; $P < 10^{-22}$, Wilcoxon signed-rank test, $n = 166$ neurons from 19 experiments).

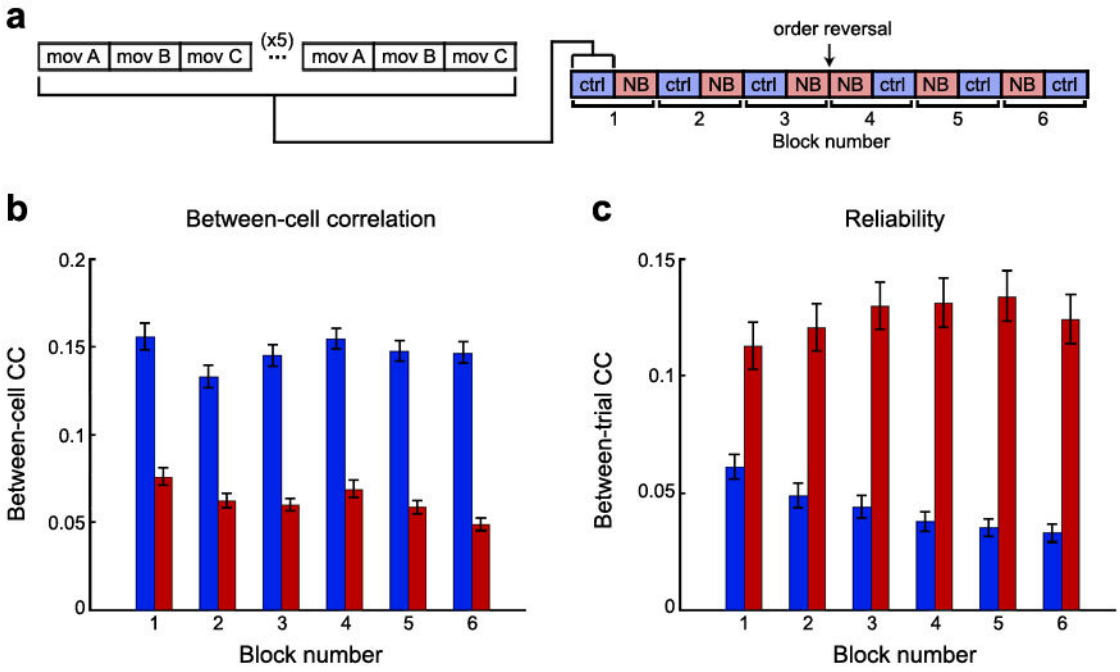

Figure 3.8: Between-cell correlation and response reliability in different stimulus blocks under both control and nucleus basalis conditions. **(a)** Schematic of movie presentation sequence. Each block consisted of 5 repeats of 3 movies. Control (ctrl, blue) and nucleus basalis stimulation (NB, red) blocks were interleaved to reduce the confounding effect of cortical adaptation induced by repeated visual stimulation. **(b)** While the between-cell CC was similar across blocks for both control and nucleus basalis conditions, CC (NB) was significantly lower than CC (control) in each of the 6 blocks. **(c)** Stimulation of nucleus basalis significantly increased between-trial CC in each of the 6 blocks, with magnitudes much larger than the differences of CC across blocks.

Furthermore, these changes could not be accounted for by the effect of repeated visual stimulus presentation, since the blocks of control and nucleus basalis trials were interleaved in the experiment (**Fig. 3.8a**), and the differences in reliability and between-cell CC across blocks were much smaller than those between the control and nucleus basalis conditions (**Fig. 3.8b,c**).

Though the effect of block order was too small to account for the difference between control and nucleus basalis conditions, there was a slight reduction of between-trial CC over control blocks (possibly caused by visual adaptation) and a slight increase of between-trial CC over nucleus basalis blocks (perhaps from enhanced ACh release induced by repeated nucleus basalis stimulation). The opposite changes of reliability over time under the control and nucleus basalis conditions further argue against the possibility that the observed effects are due to repeated presentation of the natural stimuli.

3.4 Decorrelation mediated by mAChRs

Stimulation of the nucleus basalis allows investigation into the widespread effects of cholinergic activation (see Chapter 1.5). However, the disadvantage of widespread activation, as opposed to local iontophoresis, is that stimulation of nucleus basalis might have diverse effects on cortex, as well as on non-cortical projections to the limbic system, thalamus, and brainstem. Thus, I employed pharmacological manipulations to elucidate the mechanism of nucleus basalis actions on cortical processing.

Previous studies have shown that the change in EEG pattern induced by nucleus basalis activation depends on cortical muscarinic acetylcholine receptors (mAChRs) (Metherate et al., 1992). I thus tested the role of mAChRs in nucleus basalis-induced changes in cortical responses by applying atropine sulfate, a selective mAChR antagonist, to the recording area via either intracortical injection with a micropipette (100 μM) or local application to the cortical surface (1 mM; see Online Methods).

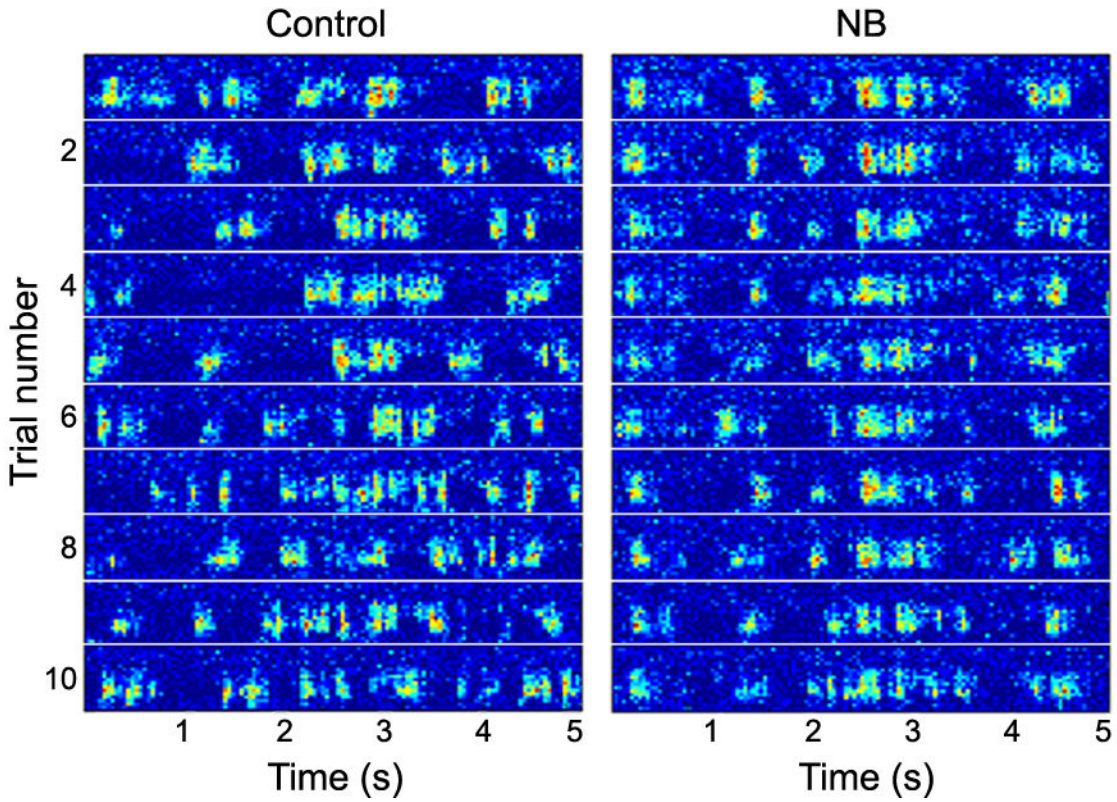

Figure 3.9: Application of mAChR antagonist diminishes nucleus basalis-induced decorrelation but does not affect increases in response reliability. An example of multiunit responses to the first 10 repeats of a movie before (Control) and after (NB) basal forebrain activation in the presence of atropine (100 μM, intracortical injection). Note that the correlation between channels was high in both control and nucleus basalis conditions, but the response was much more time-locked to the movie after nucleus basalis stimulation.

As shown in an example multiunit recording (Fig. 3.9), atropine application greatly reduced the degree of decorrelation induced by nucleus basalis stimulation. At the single unit level, although

the between-cell CC was still reduced by nucleus basalis stimulation, the magnitude of decorrelation was much smaller than that in the absence of atropine ($P < 10^{-28}$, Wilcoxon rank-sum test; n = 79 neurons from 12 experiments; Fig. 3.10a). Notably, atropine application was completely ineffective in blocking the nucleus basalis-induced increase in response reliability.

As quantified by the between-trial CC (**Fig. 3.10b**), nucleus basalis stimulation induced a highly significant increase in reliability in the presence of atropine ($P < 10^{-13}$, Wilcoxon signed-rank test; n = 79 cells from 12 experiments). In fact, compared to the recordings in the absence of atropine (**Fig. 3.4b**), the nucleus basalis-induced increase in reliability was slightly larger in the presence of atropine (**Fig. 3.10b**), although the difference was not statistically significant (P = 0.08, Wilcoxon rank-sum test).

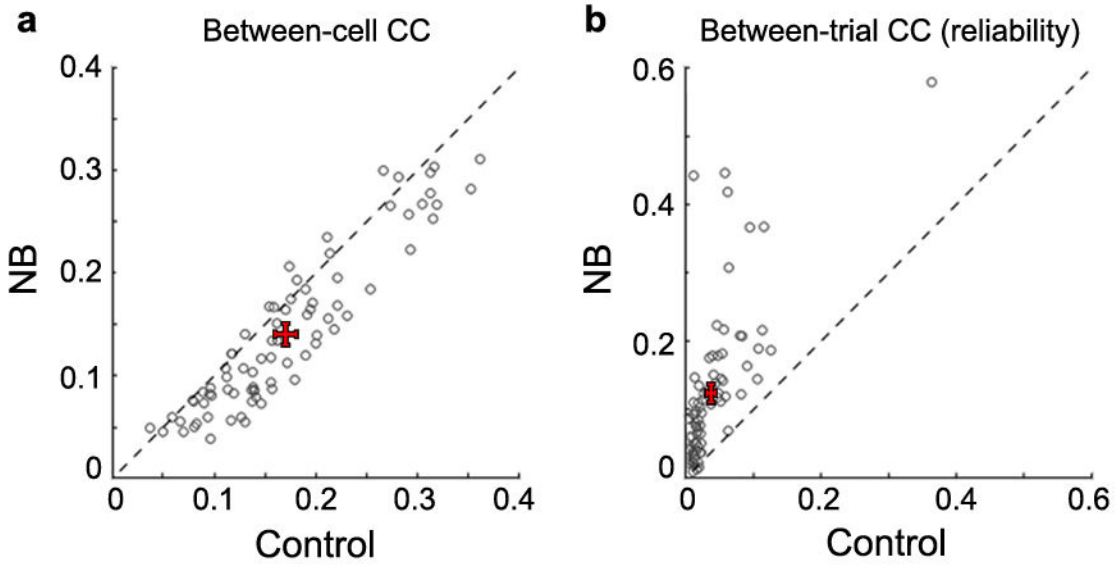

Figure 3.10: Quantification of nucleus basalis-induced effects on decorrelation and response reliability in the presence of mAChR antagonists. (**a**) Summary of between-cell CC before (Control) and after (NB) nucleus basalis stimulation in the presence of atropine (n = 79 single units from 12 experiments). (**b**) Summary of between-trial CC before (Control) and after (NB) nucleus basalis stimulation in the presence of atropine (n = 79 single units from 12 experiments).

3.5 Improved reliability involves distributed changes along the sensory pathway

The activation of mAChRs mediates the nucleus basalis-induced decorrelation of neural responses, but not the increases in response reliability. I next tested whether activation of nicotinic acetylcholine receptors (nAChRs) could underlie the increased response reliability, as nAChRs are known to enhance thalamocortical synaptic efficacy (Gil et al., 1997) and boost the visual responses of cortical neurons (Disney et al., 2007). However, a marked nucleus basalis-induced increase in response reliability was still present after cortical application of the selective nAChR antagonist mecamylamine [1 mM to 10 mM (surface application) or 100 μM to 1 mM (intracortical injection); $P < 10^{-12}$, Wilcoxon signed-rank test, n = 70 cells from 9 experiments] or Dihydro-β-erythroidine hydrobromide [DHβE, 100 μM (intracortical injection); $P < 0.001$, n = 16 cells from 3 experiments]. In the presence of these nAChR antagonists, the magnitude of the nucleus basalis-induced increase was not reduced from that observed in the absence of the

antagonists (P = 0.97, Wilcoxon rank-sum test). This suggests that nucleus basalis stimulation may have altered the visual signals before they reached V1.

To test this possibility, I made polytrode recordings in the lateral geniculate nucleus (LGN) of the thalamus (**Fig. 3.11a**, top). Indeed, single units in the LGN showed significant increases in response reliability following nucleus basalis stimulation (**Fig. 3.11b,c**; $P < 10^{-12}$, Wilcoxon signed-rank test; n = 124 cells from 9 experiments), an effect that also remained highly significant after the spike rate equalization procedure ($P < 10^{-5}$, Wilcoxon signed-rank test). This may explain why cortical AChR antagonist application was ineffective in blocking the nucleus basalis-induced increase in response reliability. Furthermore, nucleus basalis stimulation caused a significant reduction of the ratio between burst and tonic spikes in LGN activity ($P < 10^{-10}$, Wilcoxon signed-rank test; **Fig. 3.11d**). This shift from burst to tonic firing mode has been shown to increase the linearity (Sherman, 1996) and change the temporal response properties (Bezdudnaya et al., 2006) of LGN neurons, which may further shape the input to the cortex. Thus, the nucleus basalis-induced increase in response reliability is not a local effect in the cortex, but involves distributed neural circuits.

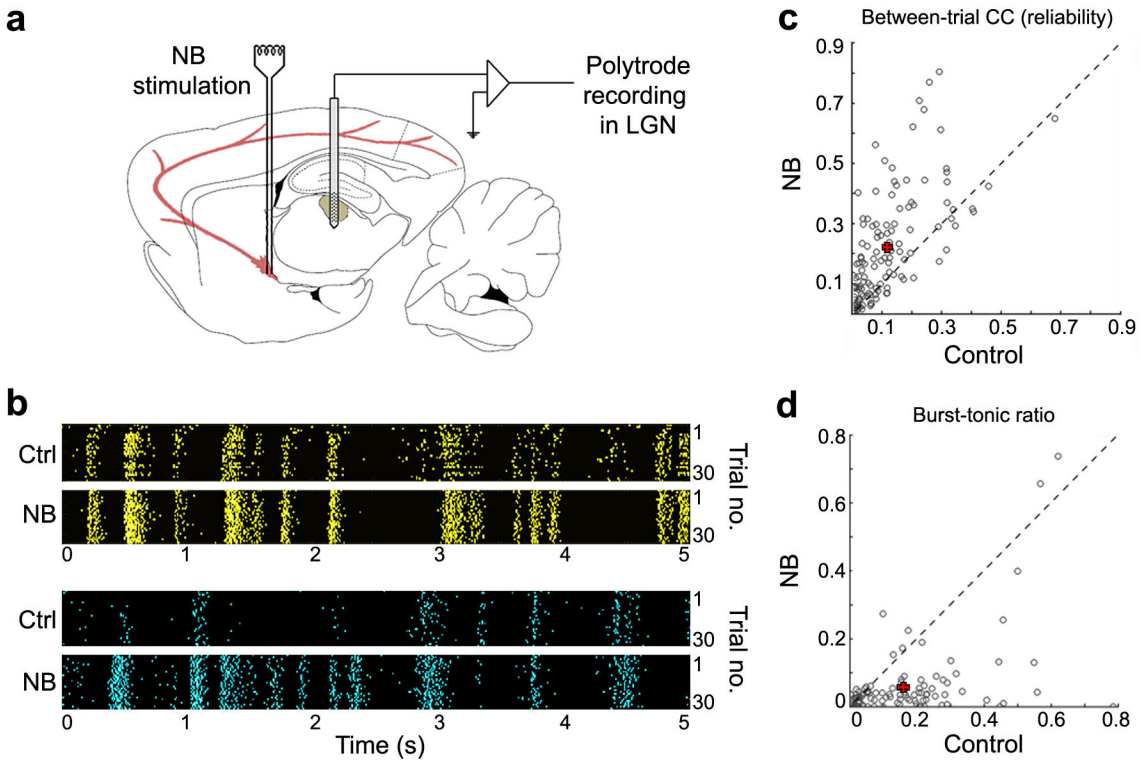

Figure 3.11: Nucleus basalis stimulation increases response reliability and shifts firing mode in the LGN. (a) Schematic illustration of experimental setup. **(b)** Responses of two example LGN single units before (Ctrl) and after (NB) nucleus basalis stimulation. Each panel shows the responses to 30 repeats of a movie. **(c)** Between-trial CC before (Control) and after (NB) nucleus basalis stimulation (n = 124 cells from 9 experiments). **(d)** Burst-tonic ratio of LGN neurons before (Control) and after (NB) nucleus basalis stimulation in the absence of visual stimulus. Each circle represents the burst-tonic ratio of one LGN neuron (n = 105 cells from 3 experiments). Error bars, ± s.e.m.

Nucleus basalis does not project directly to LGN, so the observed thalamic effects must result from indirect activation. One possibility is that nucleus baslais stimulation activates the brainstem cholinergic system [nucleus basalis receives a strong projection from the brainstem cholinergic system and there is evidence for a weaker feedback projection (McCormick, 1992; Parent et al., 1988)]. The brainstem cholinergic system has been found to modulate thalamic responses (Castro-Alamancos, 2004), and could thereby cause the observed effects. To test the possibility that the LGN effects were modulated by brainstem cholinergic input, I repeated the cortical experiments while injecting AChR antagonists into LGN (**Fig. 3.12**). The injection volume was calibrated to treat as much of the LGN as possible without going beyond its borders. Furthermore, the LGN injection electrode was bonded to a microelectrode, so that the injection site could be chosen such that the LGN multiunit receptive fields were mapped to cortical receptive fields (thereby maximizing the chances that treated neurons projected to the recorded region of cortex). However, application of atropine (100 μM) and mecamylamine (100 μM) into the LGN did not block the nucleus basalis-induced increase in cortical decorrelation ($P < 10^{-7}$, $n = 42$ cells from 4 experiments, **Fig. 3.13a**) or response reliability ($P < 10^{-7}$, $n = 42$ cells from 4 experiments, **Fig. 3.13b**), indicating that this effect is not mediated by cholinergic input to the LGN.

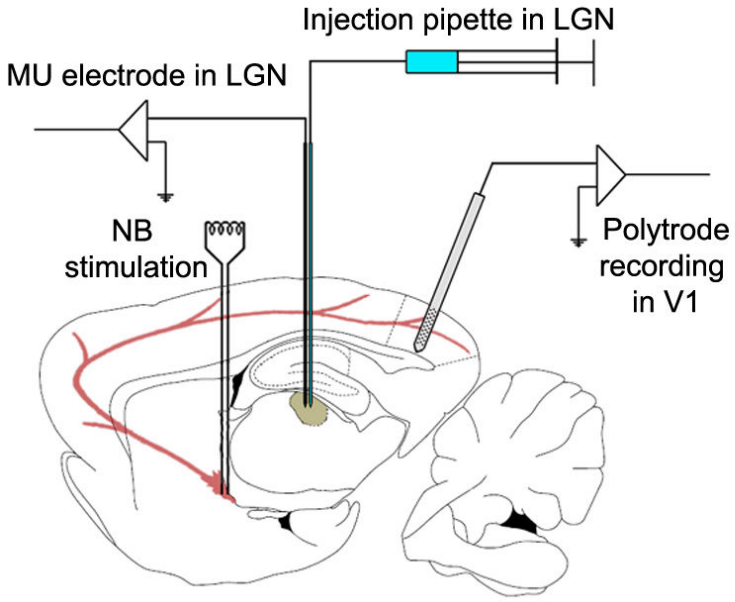

Figure 3.12: Schematic illustration of experimental setup. An injection pipette was bonded to a multi-unit recording electrode (used to map LGN multi-unit receptive field) and lowered into the LGN. Nucleus basalis stimulation and V1 polytrode recording are the same as in **Fig. 2.1**. A mixture of atropine (100 μM) and mecamylamine (100 μM) was injected into the LGN before and during the recording in V1.

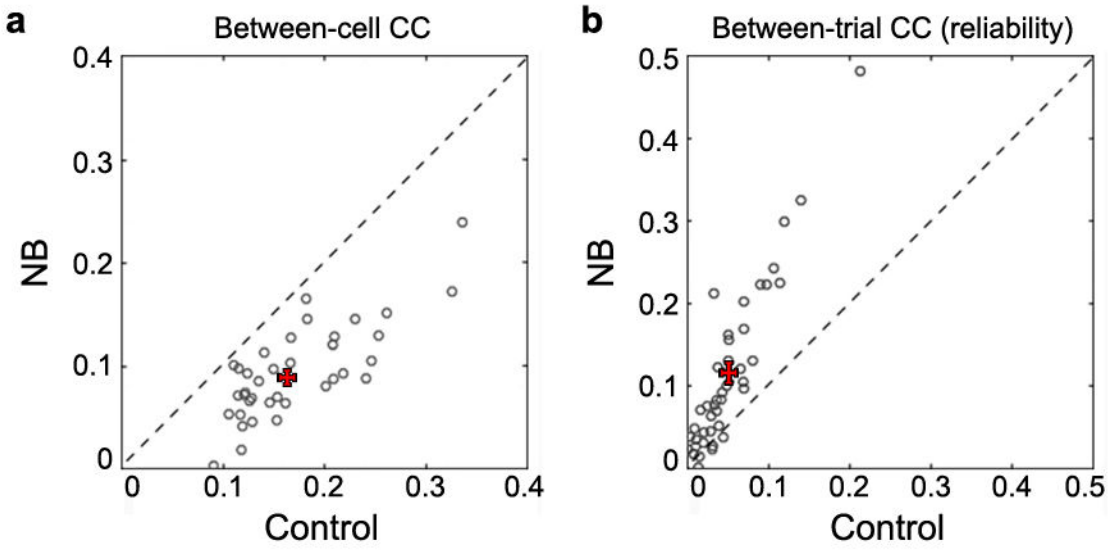

Figure 3.13: Blockade of AChRs in the LGN did not diminish nucleus basalis-induced decorrelation or increases in reliability in V1. (a) Summary of between-cell CC of V1 neurons before and after nucleus basalis stimulation with AChR blockade in the LGN. Each circle represents the average CC between a single neuron and all other neurons in the same recording. The nucleus basalis-induced decrease in between-cell CC remained highly significant ($P < 10^{-7}$, $n = 42$ cells from 4 experiments). **(b)** Summary of between-trial CC of V1 neurons before and after nucleus basalis stimulation with AChR blockade in the LGN. Each circle represents data from one neuron, averaged over CCs for all pairwise combinations of the 30 trials. The nucleus basalis-induced decrease in between-trial CC remained highly significant ($P < 10^{-7}$, $n = 42$ cells from 4 experiments). Error bars, ± s.e.m.

3.6 Basal forebrain activation enhances cortical coding of natural scenes

As discussed earlier, nucleus basalis-induced decorrelation and increased response reliability could potentially improve cortical coding of complex stimuli. Although it is not yet known how higher visual areas might utilize the output of V1 neurons, it is still possible to measure the coding fidelity of the V1 population in more abstract terms. Specifically, the fidelity of cortical encoding can be measured by determining how discriminable visual stimuli are based purely on their responses.

To investigate whether nucleus basalis stimulation increases the discriminability of natural visual stimuli, I measured the performance of an ideal observer in discriminating two stimuli (100 ms movie segments) from the population responses as a function of condition (**Fig. 3.14**). Intuitively, the ideal observer would try to determine whether a single-trial response to a stimulus had been a response to stimulus A or stimulus B based on the similarity of the single-trial response (A) to the template responses averaged across all other trials (<A> and <B>). If the single-trial response to stimulus A was closer to the template response for stimulus A [d(A,<A>) < d(A,<B>), where d is Euclidian distance], the discrimination was coded as correct, and if it was more similar to the template response for the other stimulus [d(A,<A>) < d(A,<B>)], it was coded as incorrect.

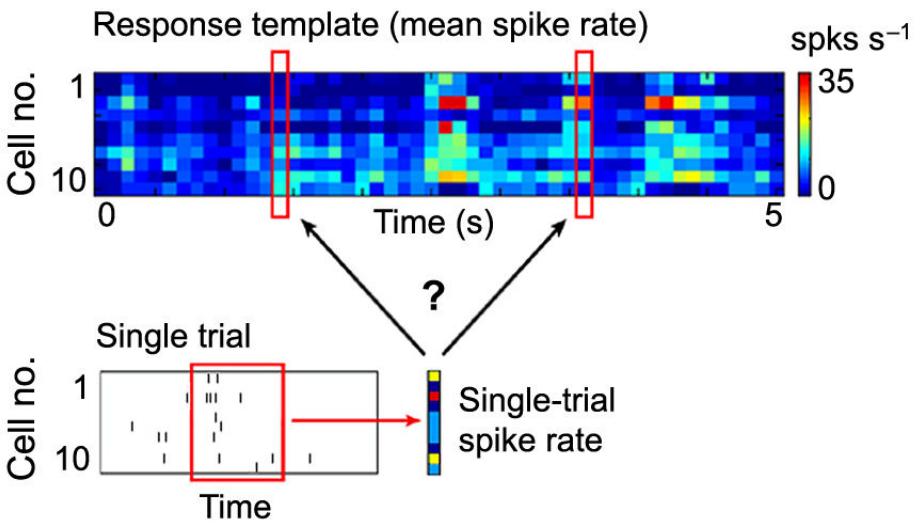

Figure 3.14: Schematic illustration of the discrimination analysis. The population response during a given stimulus segment (100 ms, red box) in each trial was classified as one of two categories based on its Euclidean distances from the two templates (population responses averaged across trials).

This was then repeated for all pairs of movie segment stimuli to measure the average discrimination of the ideal observer for each condition, as a function of population size. Comparing the nucleus basalis condition to the control condition, I found that the ideal observer performed significantly better for the responses in the nucleus basalis condition than for the responses in the control condition (**Fig. 3.15a**). This effect held true for all population sizes analyzed (N = 1 to 15 cells). This demonstrates that coding is improved in the nucleus basalis condition.

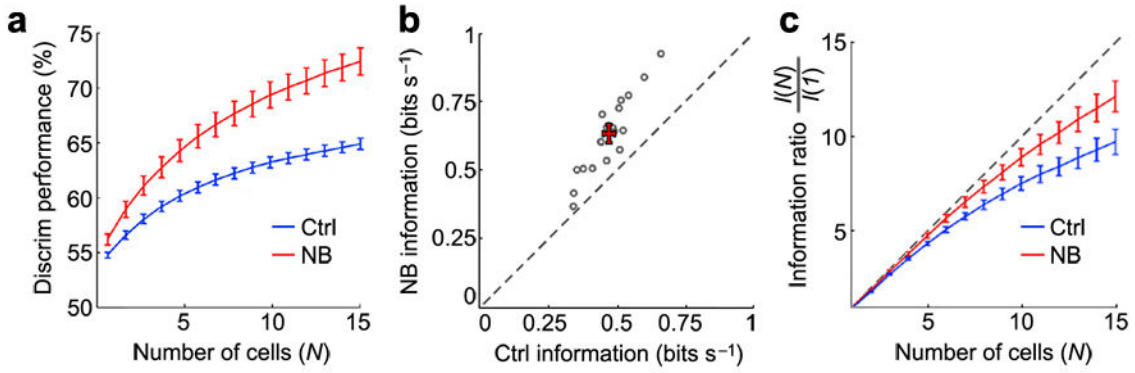

Figure 3.15: Increased reliability and decreased correlation both contribute to improved coding of natural stimuli. (a) Mean discrimination performance (% of correct classifications) as a function cell number (N) included in the population analysis for control and nucleus basalis conditions (12 experiments). **(b)** Single-neuron information [$I(1)$] before and after nucleus basalis stimulation. Each point represents $I(1)$ averaged across all cells in each experiment (19 experiments). **(c)** Information ratio [$I(N)/I(1)$] as a function of cell number (N) before and after nucleus basalis stimulation (12 experiments). Diagonal line indicates linear summation of information (no redundancy between cells). Error bars, ± s.e.m.

Next, I wanted to dissect the influence of nucleus basalis on single neuron responses (e.g., increased reliability) from the effect of nucleus basalis on between-neuron interactions (e.g., decorrelation). Using single-neuron information (see Methods), a measure unaffected by between-cell correlations, I found increased information after nucleus basalis stimulation in all 19 experiments ($P < 0.001$, Wilcoxon signed-rank test; **Fig. 3.15b**). This is likely to reflect the contribution of increased response reliability of individual neurons.

To test the effect of decorrelation on neural coding, I calculated the information ratio, defined as the total information from N cells [$I(N)$, $1 \leq N \leq 15$, averaged across all combinations of N cells in each recording] divided by the single-neuron information [$I(1)$, averaged across all single neurons in each recording]. For this measure (**Fig. 3.15c**), the ratio $I(N)/I(1)$ should be equal to N (diagonal line) if there is no redundancy between neurons. I found that in both control and nucleus basalis conditions, the ratio was lower than N, reflecting redundancy between cells. However, the redundancy was significantly reduced by nucleus basalis activation ($P < 0.05$ for $N = 7$ to 15 cells, Wilcoxon signed-rank test, with Bonferroni correction; 12 experiments). Thus, whereas the nucleus basalis-induced improvement in response reliability increased the information coded by individual neurons (**Fig. 3.15b**), the decorrelation was associated with decreased redundancy among a population of neurons (**Fig. 3.15c**).

3.7 Summary

In the current study, the role of the basal forebrain cholinergic system on cortical coding of natural scene stimuli was investigated. Stimulating nucleus basalis decorrelated neural responses while markedly increasing response reliability of individual neurons. Pharmacology experiments showed that the observed decorrelation was mediated by cortical mAChRs. The increase in response reliability was not mediated by either nAChRs or mAChRs, but instead appeared to involve nucleus basalis-induced effects on LGN, upstream in the visual pathway. Ideal observer analysis demonstrated that nucleus basalis-induced effects on both single neuron responses and between-neuron interactions led to improvement of cortical coding of natural stimuli. Taken together, these results provide the first causal evidence that basal forebrain activation can dynamically modulate cortical coding of natural sensory stimuli.

Chapter 4. Conclusions and implications

4.1 Summary of novel experimental results

Basal forebrain activation modulates cortical dynamics

Previous studies have demonstrated that nucleus basalis stimulation can act to desynchronize cortical EEG (Buzsaki et al., 1988; Metherate et al., 1992), but less is known about how nucleus basalis stimulation affects local cortical dynamics. In this study, I measured the effect of nucleus basalis stimulation on the local field potential recorded throughout the depth of cortex (Chapter 2.5). Nucleus basalis stimulation reduced low frequency oscillations (1–10 Hz) and increased the power at high frequencies (10-100 Hz), especially in the gamma frequency band (35-50 Hz). These effects were present both in the presence and absence of visual stimulation.

Effect of nucleus basalis stimulation on receptive field structure

Studies using iontophoresis of acetylcholine had found changes in cortical response properties following acetylcholine application (Muller and Singer, 1989; Roberts et al., 2005; Sato et al., 1987; Sillito and Kemp, 1983; Zinke et al., 2006), but the effects were inconsistent. Also, it was not understood how widespread cholinergic activation would affect cortical response properties, as changes in functional connectivity and local oscillatory input might have additional effects on cortical response properties (Arieli et al., 1996; Petersen et al., 2003). To address these issue, I measured orientation tuning, direction selectivity, and spatial receptive fields in the presence and absence of nucleus basalis activation (Chapter 2.6-2.7). Stimulation did not effect orientation tuning, direction selectivity, or spatial receptive field size. However, nucleus basalis stimulation did significantly increase the signal-to-noise ratio of cortical responses to visual stimulation. Taken together, these results suggest that basal forebrain activation does not affect the structure of cortical receptive fields, but does affect the gain of neural responses.

Nucleus basalis activation decorrelates single neurons and increases response reliability

The observed effects of nucleus basalis stimulation on cortical dynamics and neural gain suggested that stimulation might actively modulate responses to natural sensory stimuli in a substantive manner. However, little is known about the effect of nucleus basalis stimulation on coding of complex stimuli. In this study, repeated presentations of natural movies were shown while intermittently stimulating nucleus basalis (Chapter 3.3). Nucleus basalis stimulation acted to significantly decorrelate the responses of individual neurons, potentially improving the coding capacity of the neural population. Furthermore, nucleus basalis concomitantly increased the response reliability of single neurons, as measured by comparing single neuron responses to multiple presentations of the same movie. This effect could also potentially improve the coding of sensory stimuli by increasing response fidelity.

Effects of nucleus basalis stimualtion on decorrelation and response reliability mediated by distinct mechanisms

I next investigated the physiological mechanisms underlying the observed decorrelation and increased response reliability following nucleus basalis stimulation (Chapter 3.4-3.5). I found that the decorrelation was mediated by local cortical mAChRs, but the increased response reliability could not be blocked by application of either nAChR or mAChR antagonists. Instead, the increase in response reliability appeared to be mediated by indirect nucleus basalis-induced effects on LGN processing, upstream in the visual pathway. These results show that the effects of nucleus basalis stimulation on visual processing are mediated by distinct neural mechanisms along the sensory pathway.

Nucleus basalis stimulation improves cortical coding

Finally, I used a simple discrimination analysis to investigate whether the nucleus basalis-induced effects on cortical responses act to improve coding of sensory stimuli (Chapter 3.6). By measuring how well an ideal observer could discriminate natural scene segments based purely on the responses, I was able to quantify coding quality without making assumptions of how the information was read out by higher visual areas. I found that nucleus basalis stimulation improved ideal observer performance for a range of population sizes. I carried out further analysis to dissect stimulation effects on single neurons from stimulation effects on between-neuron interactions. By looking at the average ideal observer performance using only a single neuron, I found that effects on single neuron responses are partially responsible for the improved coding. I then normalized the single-neuron information to investigate whether stimulation effects on between-neuron interactions contributed to improved coding. Indeed, nucleus basalis stimulation reduced information redundancy between neurons, thereby improving coding across the population of neurons. These results demonstrate that nucleus basalis stimulation can dynamically enhance cortical coding of natural visual scenes.

4.2 Discussion of results

Previous studies have shown that local application of ACh or AChR agonists can affect the firing rate and receptive field properties of visual cortical neurons (Muller and Singer, 1989; Roberts et al., 2005; Sato et al., 1987; Sillito and Kemp, 1983; Zinke et al., 2006), although the observed changes were diverse across neurons and sometimes inconsistent between studies. In this study, by directly activating the source of cholinergic projections to the entire cortex, I have demonstrated two robust effects of nucleus basalis activation on visual coding, mediated by distinct mechanisms. Furthermore, I found that both the decorrelation and increased reliability contribute to improved discriminability of the neuronal responses to different natural stimuli, a hallmark of enhanced visual coding.

Effect on cortical dynamics

In this study, I found that nucleus basalis stimulation caused a reduction of low frequency activity and an increase in high frequency activity, consistent with previous research (Buzsaki et al., 1988; Metherate et al., 1992). In addition, I observed a specific band pass increase in gamma

frequency activity following nucleus basalis stimulation. The specific increase in gamma frequency activity is of interest, as gamma frequency activity has been correlated to attentional states and improved sensory processing in visual cortex (Fries et al., 2001). It is not known whether the processing is improved as a consequence of gamma frequency activity or vice versa. It is also not known how nucleus basalis stimulation induces gamma frequency activity. Activation of parvalbumin-positive interneurons has been implicated in generating and maintaining gamma frequency activity (Cardin et al., 2009; Sohal et al., 2009), but iontophoresis studies have found acetylcholine application to suppress firing of putative parvalbumin-positive interneurons (Xiang et al., 1998). This suggests either that widespread cholinergic activation has a different effect on parvalbumin-positive interneurons, or that gamma frequency activity can be induced by multiple means, and does not require activation of parvalbumin-positive interneurons. Further investigation into the generation and importance of gamma oscillations on cortical coding of sensory stimulation would help elucidate the role of gamma in arousal and attentional processing under conditions of high basal forebrain activation.

Role of nAChR and mAChR subtypes

In rat neocortex, nAChRs are expressed primarily in layer 4 (and to a lesser extent in layer 5) in both cortical neurons and thalamic terminals, whereas mAChRs (M_1–M_4) are expressed throughout the cortex, with different subtypes preferentially expressed in different layers (Zilles et al., 1989). Thalamocortical input is thought to be enhanced by nAChR activation, while excitatory intracortical synaptic activity can be suppressed by mAChRs (Gil et al., 1997; Hsieh et al., 2000). The mAChR-mediated hyperpolarization of fast-spiking interneurons may also suppress thalamocortical feedforward inhibition (Kruglikov and Rudy, 2008; Xiang et al., 1998). Based on these effects at the cellular level, a common view is that ACh enhances thalamocortical inputs but suppresses intracortical interactions (Gil et al., 1997; Hsieh et al., 2000; Kruglikov and Rudy, 2008; Oldford and Castro-Alamancos, 2003). Our finding that nucleus basalis-induced decorrelation between neurons requires local activation of mAChRs is consistent with this notion. However, while previous studies showed that activation of cortical AChRs increases the amplitude of thalamocortical input (Disney et al., 2007; Metherate and Ashe, 1993), I found that the improved response reliability was not reduced by local block of either mAChRs or nAChRs in the cortex. This indicates that the nucleus basalis-induced improvement in response reliability is not due primarily to ACh-induced increases in the amplitude of thalamocortical input, but involves changes in the sensory signals earlier in the processing pathway. Our observation is also consistent with a recent finding that iontophoretic application of ACh in the visual cortex does not reduce the trial-to-trial variability of the neuronal responses (Zinke et al., 2006).

Effect of nucleus basalis stimulation on LGN responses

Our experiments showed that nucleus basalis stimulation increases the response reliability and decreases the burst-tonic ratio of LGN neurons. Since nucleus basalis does not project directly to the LGN, these effects must be mediated by indirect pathway(s) (through either cholinergic or GABAergic projections from the nucleus basalis (NB) (Lin et al., 2006; Parent et al., 1988), such as NB $\rightarrow$ cortex $\rightarrow$ LGN, NB $\rightarrow$ thalamic reticular nucleus $\rightarrow$ LGN (McCormick, 1992; Parent et al., 1988), or NB $\rightarrow$ brainstem reticular formation $\rightarrow$ LGN (McCormick, 1992; Parent et al., 1988) (although the lack of effect of atropine and mecamylamine injected into the LGN argues

against the involvement of cholinergic projection from the reticular formation). These pathways could depolarize LGN neurons (Castro-Alamancos, 2004) and inactivate T-type Ca^{2+} channels (McCormick, 1992; Sherman, 1996), thereby increasing the response reliability and reducing the burst-tonic ratio. The changes in the LGN activity are likely to improve the fidelity of the sensory input to the cortex and thus explain the nucleus basalis-induced increase in cortical response reliability. Such distributed improvement of neuronal responses along the sensory pathway could contribute to nucleus basalis-induced enhancement of sensory cortical plasticity (Bakin and Weinberger, 1996; Kilgard and Merzenich, 1998), in addition to the local cholinergic effects in the cortex (Froemke et al., 2007). An intrinsic limitation of the extracellular stimulation technique is that it is difficult to distinguish the contributions of cholinergic and GABAergic nucleus basalis neurons and to rule out the potential activation of axons originating from other brain regions passing through the nucleus basalis. Future studies using optogenetic techniques to activate specific cell types may help to determine the role of each cell type in regulating sensory coding along the thalamocortical pathway (Zhang et al., 2007).

Implications

The activity of cholinergic neurons in the basal forebrain undergoes striking changes from the sleep to awake states (Jones, 2004; Lee et al., 2005; Parikh et al., 2007). Recent studies showed that even in the awake state, nucleus basalis activity varies in a task-dependent manner (Laplante et al., 2005; Parikh et al., 2007), and it may be involved in regulating sensory processing under different forms of uncertainty (Yu and Dayan, 2005). Since nucleus basalis receives input from both subcortical regions and prefrontal cortex (Sarter et al., 2005), it may act as a way station for both bottom-up and top-down signals to regulate sensory coding in a behaviorally-relevant manner. Our finding that nucleus basalis activation can rapidly improve visual representation in the cortex offers a mechanism by which perceptual abilities are enhanced during wakefulness, arousal, and attention.

4.3 Future directions

Awake-restrained recording

The above findings suggest that nucleus basalis dynamically modulates sensory processing in the anesthetized animal. The cholinergic neurons of the nucleus basalis are known to be active in a tonic manner during waking and REM sleep, but not during slow wave sleep (Jones, 2004; Lee et al., 2005). Furthermore, in awake animals nucleus basalis is active at high firing rates in a task-dependent manner (Laplante et al., 2005; Parikh et al., 2007). This suggests that endogenous modulation of nucleus basalis activity may underlie improved sensory processing during states of wakefulness, arousal, and attention. However, further reseach is necessary to determine whether endogenous modulation of nucleus basalis activity is sufficient to drive changes in cortical coding in the awake animal.

To investigate this possibility, the experimental approach will need to be extended to an awake-restrained preparation. This will allow quantitative measurement of cortical responses while displaying carefully controlled visual stimuli to the animal. An experimental preparation has been developed for recording from awake-restrained rodents with minimal stress to the animal (**Fig 4.1**) (Dombeck et al., 2007). Specifically, the animal is held by a surgically implanted head

plate and placed on the top of a spherical treadmill. The treadmill is constructed from a lightweight ball floated on air in a hemispherical container fixed to the recording table. This allows the animal to run freely without disrupting the neural recordings.

Recording endogenous nucleus basalis activity

To test the role of endogenous modulation of nucleus activity, a recording electrode (or array) would be placed in nucleus basalis and a polytrode would be placed in area V1. The multiunit activity would be measured in nucleus basalis as the animal observed multiple trials of a natural movie or noise stimulus. Thereby, the response properties of single nuerons and the coding fidelity of the population could be compared during periods of high and low endogenous nucleus basalis activity. This experiment would allow investigation into the effects of endogenous nucleus basalis modulation on cortical processing. However, it would not provide a causal link, as both nucleus basalis activity and cortical processing could have been upregulated by an upstream ascending system (e.g., brainstem cholinergic system).

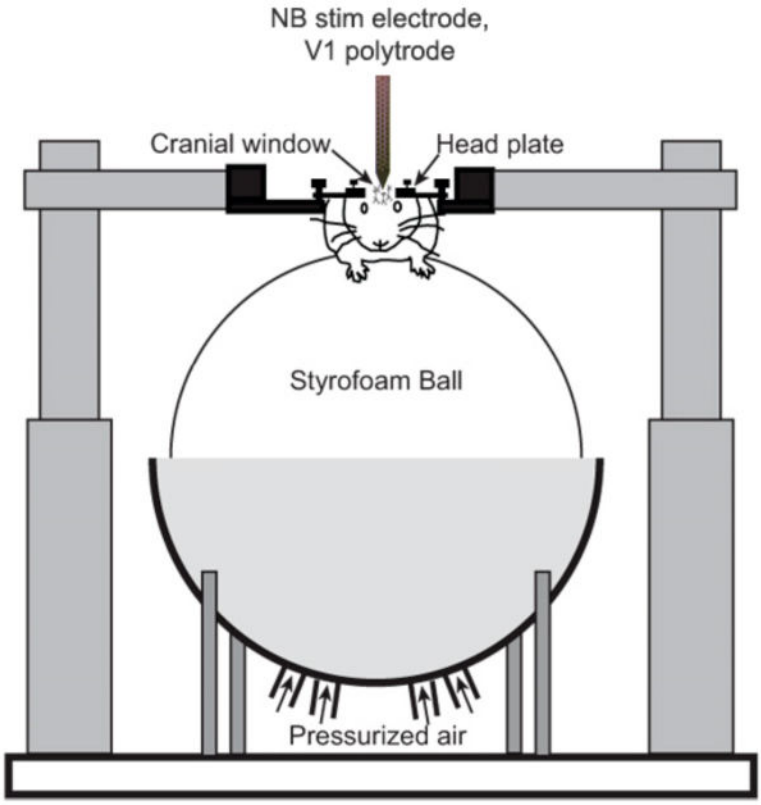

Figure 4.1: Schematic illustration of the awake-restrained recording. The spherical treadmill allows animals to move freely without disrupting stimulation or recording. Adapted from Dombeck et al. (Dombeck et al., 2007).

Electrically inducing endogenous levels of nucleus basalis activity

To determine whether endogenous levels of high nucleus basalis activity have an effect on cortical processing, it will be necessary to activate the nucleus basalis in a systematic fashion,

and compare coding in the activated trials to the control trials. The recordings from nucleus basalis would provide an estimate of firing rates during periods of high endogenous activation. This level could then be induced experimentally by calibrating the electrical stimulation of the nucleus basalis to drive activity at high endogenous levels. If this stimulation drove changes in cortical coding, it would provide strong causal evidence that nucleus basalis modulates cortical processing in the awake animal, and thereby plays a role in perceptual improvements during states of wakefulness, arousal, and attention.

Optogenetically inducing endogenous levels of nucleus basalis activity

An alternative approach to stimulating nucleus basalis in the awake animal would be to use optogenetic techniques to selectively activate the relevant neurons with laser illumination (Zhang et al., 2007). Transgenic mice expressing channelrhodopsin-2 (Boyden et al., 2005) under a choline acetyltransferase (ChAT) promoter would be implanted with an optic fiber in the basal forebrain, allowing selective excitation of the cholinergic neurons in the nucleus basalis (**Fig. 4.2**). This approach has two major advantages over traditional electrical stimulation.

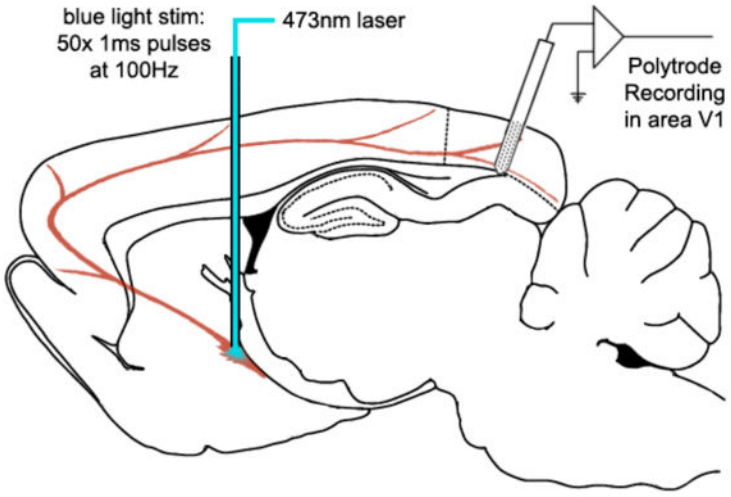

Figure 4.2: Schematic illustration of optogenetic activation of nucleus basalis. Blue light illumination would be delivered to the basal forebrain by an optic fiber fed through an implanted cannula. This would allow selective activation of cholinergic cells of the basal forebrain. Polytrode recording as in Fig. 1.1.

First, since only the cholinergic neurons would be activated, it would exclude any effect of activating non-cholinergic cells or fibers of passage. Second, electrical stimulation activates cells in a somewhat unrealistic manner, driving them in a highly synchronous manner, as well as driving all cells near the electrode regardless of their membrane potential at the time of stimulation. In contrast, low levels of light delivery could act to depolarize cholinergic nucleus basalis cells in a tonic manner until the desired firing rate was achieved. This would avoid highly synchronous and nonselective activation, and would instead induce firing patterns more similar to endogenous states of high nucleus basalis activation.

Conclusion

The role of the basal forebrain cholinergic system in sensory processing is but one example of the manner in which modulation of information processing circuits may underlie cognitive phenomena of interest. New technical advances such as large scale multi-electrode recording, 2-photon imaging of activity-sensitive dyes, and optogenetic manipulation of genetically-defined cell populations will increasingly allow the systematic dissection of modulatory actions upon neural circuits. This includes not only segregated neurotransmitter-specific systems like the basal forebrain cholinergic projection, but also smaller sub-networks of neurons (or even glia) embedded within larger information processing structures. Systematic manipulation of information processing circuits will be an essential approach to understanding the underpinnings of cognitive and perceptual phenomena.

References

Arieli, A., Sterkin, A., Grinvald, A., and Aertsen, A. (1996). Dynamics of ongoing activity: explanation of the large variability in evoked cortical responses. Science *273*, 1868-1871.

Bakin, J. S., and Weinberger, N. M. (1996). Induction of a physiological memory in the cerebral cortex by stimulation of the nucleus basalis. Proc Natl Acad Sci U S A *93*, 11219-11224.

Barlow, H. B. (1953). Summation and inhibition in the frog's retina. J Physiol *119*, 69-88.

Berger, H. (1929). Electroencephalogram in humans. Archiv Fur Psychiatrie Und Nervenkrankheiten *87*, 527-570.

Bezdudnaya, T., Cano, M., Bereshpolova, Y., Stoelzel, C. R., Alonso, J. M., and Swadlow, H. A. (2006). Thalamic burst mode and inattention in the awake LGNd. Neuron *49*, 421-432.

Blanche, T. J., Spacek, M. A., Hetke, J. F., and Swindale, N. V. (2005). Polytrodes: high-density silicon electrode arrays for large-scale multiunit recording. J Neurophysiol *93*, 2987-3000.

Boyden, E. S., Zhang, F., Bamberg, E., Nagel, G., and Deisseroth, K. (2005). Millisecond-timescale, genetically targeted optical control of neural activity. Nat Neurosci *8*, 1263-1268.

Buzsaki, G., Bickford, R. G., Ponomareff, G., Thal, L. J., Mandel, R., and Gage, F. H. (1988). Nucleus basalis and thalamic control of neocortical activity in the freely moving rat. J Neurosci *8*, 4007-4026.

Cardin, J. A., Carlen, M., Meletis, K., Knoblich, U., Zhang, F., Deisseroth, K., Tsai, L. H., and Moore, C. I. (2009). Driving fast-spiking cells induces gamma rhythm and controls sensory responses. Nature *459*, 663-667.

Castro-Alamancos, M. A. (2004). Dynamics of sensory thalamocortical synaptic networks during information processing states. Prog Neurobiol *74*, 213-247.

Disney, A. A., Aoki, C., and Hawken, M. J. (2007). Gain modulation by nicotine in macaque v1. Neuron *56*, 701-713.

Dombeck, D. A., Khabbaz, A. N., Collman, F., Adelman, T. L., and Tank, D. W. (2007). Imaging large-scale neural activity with cellular resolution in awake, mobile mice. Neuron *56*, 43-57.

Everitt, B. J., and Robbins, T. W. (1997). Central cholinergic systems and cognition. Annu Rev Psychol *48*, 649-684.

Felsen, G., Touryan, J., Han, F., and Dan, Y. (2005). Cortical sensitivity to visual features in natural scenes. PLoS Biol *3*, e342.

Fries, P., Reynolds, J. H., Rorie, A. E., and Desimone, R. (2001). Modulation of oscillatory neuronal synchronization by selective visual attention. Science *291*, 1560-1563.

Froemke, R. C., Merzenich, M. M., and Schreiner, C. E. (2007). A synaptic memory trace for cortical receptive field plasticity. Nature *450*, 425-429.

Gil, Z., Connors, B. W., and Amitai, Y. (1997). Differential regulation of neocortical synapses by neuromodulators and activity. Neuron *19*, 679-686.

Girman, S. V., Sauve, Y., and Lund, R. D. (1999). Receptive field properties of single neurons in rat primary visual cortex. J Neurophysiol *82*, 301-311.

Goard, M., and Dan, Y. (2009). Basal forebrain activation enhances cortical coding of natural scenes. Nat Neurosci.

Hazan, L., Zugaro, M., and Buzsaki, G. (2006). Klusters, NeuroScope, NDManager: a free software suite for neurophysiological data processing and visualization. J Neurosci Methods *155*, 207-216.

Heimel, J. A., Van Hooser, S. D., and Nelson, S. B. (2005). Laminar organization of response properties in primary visual cortex of the gray squirrel (Sciurus carolinensis). J Neurophysiol *94*, 3538-3554.

Herrero, J. L., Roberts, M. J., Delicato, L. S., Gieselmann, M. A., Dayan, P., and Thiele, A. (2008). Acetylcholine contributes through muscarinic receptors to attentional modulation in V1. Nature *454*, 1110-1114.

Hsieh, C. Y., Cruikshank, S. J., and Metherate, R. (2000). Differential modulation of auditory thalamocortical and intracortical synaptic transmission by cholinergic agonist. Brain Res *880*, 51-64.

Hubel, D. H., and Wiesel, T. N. (1961). Integrative action in the cat's lateral geniculate body. J Physiol *155*, 385-398.

Hubel, D. H., and Wiesel, T. N. (1962). Receptive fields, binocular interaction and functional architecture in the cat's visual cortex. J Physiol *160*, 106-154.

Jones, B. E. (2004). Activity, modulation and role of basal forebrain cholinergic neurons innervating the cerebral cortex. Prog Brain Res *145*, 157-169.

Jones, B. E. (2008). Modulation of cortical activation and behavioral arousal by cholinergic and orexinergic systems. Ann N Y Acad Sci *1129*, 26-34.

Jones, J. P., and Palmer, L. A. (1987). The two-dimensional spatial structure of simple receptive fields in cat striate cortex. J Neurophysiol *58*, 1187-1211.

Kara, P., Reinagel, P., and Reid, R. C. (2000). Low response variability in simultaneously recorded retinal, thalamic, and cortical neurons. Neuron *27*, 635-646.

Katzner, S., Nauhaus, I., Benucci, A., Bonin, V., Ringach, D. L., and Carandini, M. (2009). Local origin of field potentials in visual cortex. Neuron *61*, 35-41.

Kilgard, M. P., and Merzenich, M. M. (1998). Cortical map reorganization enabled by nucleus basalis activity. Science *279*, 1714-1718.

Kimura, F., Fukuda, M., and Tsumoto, T. (1999). Acetylcholine suppresses the spread of excitation in the visual cortex revealed by optical recording: possible differential effect depending on the source of input. Eur J Neurosci *11*, 3597-3609.

Kruglikov, I., and Rudy, B. (2008). Perisomatic GABA release and thalamocortical integration onto neocortical excitatory cells are regulated by neuromodulators. Neuron *58*, 911-924.

Laplante, F., Morin, Y., Quirion, R., and Vaucher, E. (2005). Acetylcholine release is elicited in the visual cortex, but not in the prefrontal cortex, by patterned visual stimulation: a dual in vivo microdialysis study with functional correlates in the rat brain. Neuroscience *132*, 501-510.

Lee, M. G., Hassani, O. K., Alonso, A., and Jones, B. E. (2005). Cholinergic basal forebrain neurons burst with theta during waking and paradoxical sleep. J Neurosci *25*, 4365-4369.

Lehmann, J., Nagy, J. I., Atmadia, S., and Fibiger, H. C. (1980). The nucleus basalis magnocellularis: the origin of a cholinergic projection to the neocortex of the rat. Neuroscience *5*, 1161-1174.

Lin, S. C., Gervasoni, D., and Nicolelis, M. A. (2006). Fast modulation of prefrontal cortex activity by basal forebrain noncholinergic neuronal ensembles. J Neurophysiol *96*, 3209-3219.

Marmarelis, V. Z. (1977). A family of quasi-white random signals and its optimal use in biological system identification. Part I: theory. Biol Cybern *27*, 49-56.

Marmarelis, V. Z., and McCann, G. D. (1977). A family of quasi-white random signals and its optimal use in biological system identification. Part II: application to the photoreceptor of Calliphora erythrocephala. Biol Cybern *27*, 57-62.

McCormick, D. A. (1992). Neurotransmitter actions in the thalamus and cerebral cortex and their role in neuromodulation of thalamocortical activity. Prog Neurobiol *39*, 337-388.

McLin, D. E., 3rd, Miasnikov, A. A., and Weinberger, N. M. (2002). The effects of electrical stimulation of the nucleus basalis on the electroencephalogram, heart rate, and respiration. Behav Neurosci *116*, 795-806.

Metherate, R., and Ashe, J. H. (1993). Nucleus basalis stimulation facilitates thalamocortical synaptic transmission in the rat auditory cortex. Synapse *14*, 132-143.

Metherate, R., Cox, C. L., and Ashe, J. H. (1992). Cellular bases of neocortical activation: modulation of neural oscillations by the nucleus basalis and endogenous acetylcholine. J Neurosci *12*, 4701-4711.

Muir, J. L., Everitt, B. J., and Robbins, T. W. (1994). AMPA-induced excitotoxic lesions of the basal forebrain: a significant role for the cortical cholinergic system in attentional function. J Neurosci *14*, 2313-2326.

Muller, C. M., and Singer, W. (1989). Acetylcholine-induced inhibition in the cat visual cortex is mediated b7 a GABAergic mechanism. Brain Res *487*, 335-342.

Niell, C. M., and Stryker, M. P. (2008). Highly selective receptive fields in mouse visual cortex. J Neurosci *28*, 7520-7536.

Oldford, E., and Castro-Alamancos, M. A. (2003). Input-specific effects of acetylcholine on sensory and intracortical evoked responses in the "barrel cortex" in vivo. Neuroscience *117*, 769-778.

Page, K. J., Everitt, B. J., Robbins, T. W., Marston, H. M., and Wilkinson, L. S. (1991). Dissociable effects on spatial maze and passive avoidance acquisition and retention following AMPA- and ibotenic acid-induced excitotoxic lesions of the basal forebrain in rats: differential dependence on cholinergic neuronal loss. Neuroscience *43*, 457-472.

Parent, A., Pare, D., Smith, Y., and Steriade, M. (1988). Basal forebrain cholinergic and noncholinergic projections to the thalamus and brainstem in cats and monkeys. J Comp Neurol *277*, 281-301.

Parikh, V., Kozak, R., Martinez, V., and Sarter, M. (2007). Prefrontal acetylcholine release controls cue detection on multiple timescales. Neuron *56*, 141-154.

Paxinos, G., and Watson, C. (1998). The rat brain in stereotaxic coordinates, 4th edn (San Diego, Academic Press).

Penfield, W., and Erickson, T. C. (1941). Epilepsy and cerebral localization; a study of the mechanism, treatment and prevention of epileptic seizures, "First edition." edn (Springfield, Ill., Baltimore, Md.,, C. C. Thomas).

Petersen, C. C., Hahn, T. T., Mehta, M., Grinvald, A., and Sakmann, B. (2003). Interaction of sensory responses with spontaneous depolarization in layer 2/3 barrel cortex. Proc Natl Acad Sci U S A *100*, 13638-13643.

Poulet, J. F., and Petersen, C. C. (2008). Internal brain state regulates membrane potential synchrony in barrel cortex of behaving mice. Nature *454*, 881-885.

Prusky, G. T., West, P. W., and Douglas, R. M. (2000). Behavioral assessment of visual acuity in mice and rats. Vision Res *40*, 2201-2209.

Reid, R. C., and Alonso, J. M. (1995). Specificity of monosynaptic connections from thalamus to visual cortex. Nature *378*, 281-284.

Roberts, M. J., Zinke, W., Guo, K., Robertson, R., McDonald, J. S., and Thiele, A. (2005). Acetylcholine dynamically controls spatial integration in marmoset primary visual cortex. J Neurophysiol *93*, 2062-2072.

Sanchez-Vives, M. V., and McCormick, D. A. (2000). Cellular and network mechanisms of rhythmic recurrent activity in neocortex. Nat Neurosci *3*, 1027-1034.

Sarter, M., Hasselmo, M. E., Bruno, J. P., and Givens, B. (2005). Unraveling the attentional functions of cortical cholinergic inputs: interactions between signal-driven and cognitive modulation of signal detection. Brain Res Brain Res Rev *48*, 98-111.

Sato, H., Hata, Y., Masui, H., and Tsumoto, T. (1987). A functional role of cholinergic innervation to neurons in the cat visual cortex. J Neurophysiol *58*, 765-780.

Sharpee, T. O., Sugihara, H., Kurgansky, A. V., Rebrik, S. P., Stryker, M. P., and Miller, K. D. (2006). Adaptive filtering enhances information transmission in visual cortex. Nature *439*, 936-942.

Sherman, S. M. (1996). Dual response modes in lateral geniculate neurons: mechanisms and functions. Vis Neurosci *13*, 205-213.

Sillito, A. M., and Kemp, J. A. (1983). Cholinergic modulation of the functional organization of the cat visual cortex. Brain Res *289*, 143-155.

Sohal, V. S., Zhang, F., Yizhar, O., and Deisseroth, K. (2009). Parvalbumin neurons and gamma rhythms enhance cortical circuit performance. Nature *459*, 698-702.

van Hateren, J. H., and Ruderman, D. L. (1998). Independent component analysis of natural image sequences yields spatio-temporal filters similar to simple cells in primary visual cortex. Proc Biol Sci *265*, 2315-2320.

Wilson, M. A., and McNaughton, B. L. (1993). Dynamics of the hippocampal ensemble code for space. Science *261*, 1055-1058.

Worgotter, F., Suder, K., Zhao, Y., Kerscher, N., Eysel, U. T., and Funke, K. (1998). State-dependent receptive-field restructuring in the visual cortex. Nature *396*, 165-168.

Xiang, Z., Huguenard, J. R., and Prince, D. A. (1998). Cholinergic switching within neocortical inhibitory networks. Science *281*, 985-988.

Yu, A. J., and Dayan, P. (2005). Uncertainty, neuromodulation, and attention. Neuron *46*, 681-692.

Zhang, F., Aravanis, A. M., Adamantidis, A., de Lecea, L., and Deisseroth, K. (2007). Circuit-breakers: optical technologies for probing neural signals and systems. Nat Rev Neurosci *8*, 577-581.

Zilles, K., Schroder, H., Schroder, U., Horvath, E., Werner, L., Luiten, P. G., Maelicke, A., and Strosberg, A. D. (1989). Distribution of cholinergic receptors in the rat and human neocortex. Exs *57*, 212-228.

Zinke, W., Roberts, M. J., Guo, K., McDonald, J. S., Robertson, R., and Thiele, A. (2006). Cholinergic modulation of response properties and orientation tuning of neurons in primary visual cortex of anaesthetized Marmoset monkeys. Eur J Neurosci *24*, 314-328.